



Department of Astronomy, Albanova

Identifying Population III galaxies in the early Universe

using the next-generation telescopes JWST & WISH

Simon Eriksson

June 1, 2014

BSc Thesis in cooperation with
supervisor: Erik Zackrisson

Abstract

The interest in and search for the very first stars and galaxies continues to increase, as theoretical models, simulations and possible detection methods collectively improve and converge towards the promise of a discovery. Being the first stars, their importance for astrophysics and cosmology is hard to overstate, and they hold the key to understanding how matter in the Universe evolved to form the galaxies, stars and planets we see today.

In this work I investigate a promising new method, which will hopefully aid in the detection and identification of gravitationally lensed Population III galaxies at high redshifts. The main goal is to be able to distinguish the much sought after IMF of these first stars, from a range of stellar models. I present a functional data selection process, utilizing models from the Yggdrasil population synthesis code (Zackrisson et al. 2011), and go on to investigate the effects on the model, of complicating factors such as circumstellar nebular gas emissions and the inclusion of extremely metal-poor stellar models. I conclude that the method is viable for use with surveys from the next-generation telescopes JWST & WISH. However, for it to be successful, it requires specific circumstances, such as extreme gravitational lensing and higher than currently predicted stellar population masses.

Contents

1	Introduction	1
1.1	Pop III stars	4
1.1.1	The Pop III stellar IMF	4
1.1.2	Pop III galaxies	6
1.2	Gravitational lensing	7
1.3	The WISH mission	10
1.4	The James Webb Space Telescope	10
1.5	The Yggdrasil population synthesis code	11
2	Results	15
2.1	Selecting the optimal redshift and filter combination	15
2.1.1	Lyman break at 1216 Å limits filter selection	15
2.1.2	Filter performance depends on redshift	16
2.1.3	Finding the optimal filter combination	19
2.2	Adding nebular gas cloud emissions	21
2.3	Including EMP galaxy models for WISH	24
2.4	Final WISH results	25
2.4.1	The drawbacks of a 3σ S/N	26
2.5	Final JWST/NIRCam results	27
2.5.1	Improving the measurements	29
3	Discussion	30
	Acknowledgements	32
	References	33
	Appendix: Python Code Example	35

1 Introduction

With this work I endeavour to shed some light on the possibilities of using two upcoming infrared deep space telescope missions to detect the very first stars that formed in the Universe – so called Population III stars. Being able to discern these stars from the subsequent generations of stars might tell us something about their properties, e.g. the typical stellar mass. But before we delve into the specifics of what a Population III star actually is, I first want to place them in the proper context, by presenting a brief history of the early Universe. Following the Big Bang 13.8 billion years ago (Planck Collaboration 2013), the Universe started cooling as it expanded at incredible rates. Eventually the density and temperature of the Universe decreased to a point where it became transparent to photons, the force carrier particles of the electromagnetic force – or what we commonly refer to as light. This change in the state of the Universe occurred around 380,000 years ago and was marked by the release of the Cosmic Microwave Background (CMB). The photons of which permeate the seemingly infinite Universe, to such an extent that if one accounts for all the photons ever produced in stars, these would only contribute a few percent to the average energy density of radiation in the Universe.

After this point in time however, and for about 100 million years (Myr) thereafter, the Universe was a cold and dark place consisting of mostly neutral hydrogen and helium gas where the only light was the ever darkening glow from the CMB. With time, this gas coalesced into the first stars and galaxies, at locations with high densities of, most likely 'cold' (non-relativistic), dark matter (CDM). These stars and galaxies are commonly defined as belonging to 'Population III' (henceforth 'Pop III'). This classification is primarily related to the *metallicity* (Z) of a star, i.e. what fraction of the stellar mass is made up of elements heavier than hydrogen and helium. Due to the fact that essentially no elements heavier than helium, save trace amounts of lithium, were produced during the Big Bang, a Pop III star is defined as having $Z = 0$. To the best of our knowledge, none of these objects still exist in the Universe around us. In section 1.1 I will go into further detail regarding the properties of Pop III stars and galaxies, their formation and characteristics.

The stars we do see are divided into two groups – Pop II and Pop I, where Pop II represents 'metal poor' stars, with a metallicity of $Z \sim 10^{-4}$ (Karlsson et al 2013), most of which have been around for a long time, and some are up to 13.5 billion years old. They are generally found in the centre of spiral galaxies or in elliptical galaxies, but even in 'globular clusters' that e.g. orbit the Milky Way, above and around the galactic plane (Karlsson 2009). The Sun on the other hand is a Pop I star, with a fairly high fraction of heavy elements, $Z = 0.013$ (Asplund et al. 2009), and like most other

Pop I stars in our galaxy, it is located in the galactic disk of dust and gas where star formation still takes place.

Now that we have established *what* a Pop III star is, *why* are people so interested in finding them, other than out of sheer curiosity? To answer that question, let us first take a look at the Universe today, and compare it with that cold, dark and neutral place I mentioned earlier. In the present Universe, the gas outside of galaxies and galaxy clusters – the *intergalactic medium* (IGM), is actually very hot ($\sim 10^4$ K). One might expect that only areas where stars and galaxies formed would become natural 'hot spots' when compared to the rest of the Universe, but it also appears that some process transformed the IGM from a neutral and relatively cold state, to a hot, ionized state. This is called the *reionization* of the Universe, and is believed to have taken place between 100 Myr and 800 Myr after the Big Bang, or at a redshift of $7 < z < 30$ (Barkana & Loeb 2001). It is believed that Pop III stars played a crucial role in initializing this process, and as such they are a key component in improving our understanding of it.

It also appears that in the heart of essentially every large galaxy, there lurks a *supermassive black hole* (SMBH) with the most massive ones having a mass in the $\sim 10^{10} M_{\odot}$ range. The origin of these behemoths remain an open question and while early theories centred on a hierarchical growth over time through the mergers of galaxies, recent research proves the existence of quasar SMBHs in this mass range in galaxies at $z \sim 7$ (Mortlock et al. 2011). The indication of SMBHs of this mass at such a early time in the history of the Universe makes them even more of a mystery, since a hierarchical growth through the mergers of galaxies would require more time. Pop III stars and their remnants are now considered to represent a possible source of the initial seeds that could lead to SMBH formation. Whalen & Fryer (2012) investigate this possibility, for the Pop III IMF that is currently in favour (more on this in section 1.1.1). They find that with an IMF where the stellar mass is lower, $20\text{-}40 M_{\odot}$, than the previously favoured model ($\sim 100 M_{\odot}$), SMBHs are far less likely to form from these lower-mass Pop III stars than more massive ones. There are also theories that SMBHs could have formed from a 'direct collapse' of gas clouds (Tanaka & Li 2014).

Another aspect of the importance of Pop III stars relates to how the Universe has evolved chemically following the Big Bang, and as such, how our own Sun and the Earth were able to form and thus ultimately affected how we ourselves came to exist. Elements heavier than hydrogen and up to iron/nickel are formed in stellar nucleosynthesis, i.e. the process of fusion that takes place in stars. Heavier elements than this are believed to form in supernovae or other, even more energetic events. Since Pop III stars started out with $Z = 0$ and are believed to have been massive enough (see section 1.1) to carry the stellar nucleosynthesis to its conclusion, i.e. a iron/nickel

core and a subsequent supernovae explosion, they were instrumental in seeding the Universe with the very first elements, other than hydrogen/helium.

The most important first step in understanding Pop III stars, and as such learning more about the above, is understanding what their *initial mass function* (IMF) looks like. The mass of a star is very closely related to how the star evolves and what properties it has, so understanding the IMF allows you to discern one population of stars from another. The various IMF models will be discussed further in section 1.1.1.

What I attempt to do in this thesis work is to investigate if it might become possible to discern one IMF from another, based on the stellar spectral properties of stars with a specific IMF, using the next generation of infrared telescopes – the Wide-field Imaging Surveyor for High-redshift (WISH) and the James Webb Space Telescope (JWST). On their own, these telescopes will not be able to detect Pop III galaxies, let alone individual Pop III stars, simply because these objects are much too far away, and thus much too faint to fall within the detection limits of WISH or JWST. Rydberg et al. (2013) reach this conclusion when investigating the likelihood of being able to detect individual Pop III stars with JWST. Even if one accounts for gravitational lensing with flux magnification factors of up to ~ 100 , the *star formation rate* (SFR) would need to be significantly higher than what one might realistically hope, for JWST to be able to detect a single Pop III star. With that in mind, an obvious question is: Why should I even bother with looking into this with an outset that looks fairly bleak?

The premise of my work comes down to this: If it is possible to find gravitational lenses with a flux magnification greater than 100 for 'small' objects (see section 1.2), Pop III galaxies, which essentially are Pop III star clusters surrounded by a dark matter halo, with a stellar mass of $\sim 10^4 M_{\odot}$, could come within the detection thresholds for WISH and JWST. The *spectral energy distribution* (SED) from such a 'galaxy' could be compared to known Pop I and Pop II IMFs in an attempt to discern which Pop III models are most likely. Additionally I will attempt to include models of *extremely metal poor* (EMP) stars and see how they conflict with the possible signatures of Pop III stars. This is relevant since EMP stars have exceedingly low metallicities, $10^{-5} < Z < 10^{-7}$ (Yong et al. 2013), and could therefore have very similar properties to Pop III stars if they share a similar IMF. More details on all this and the actual method used will follow in the coming sections.

1.1 Pop III stars

The formation of these first stars is believed to have happened in CDM 'minihalos' with a mass of $\sim 10^5 - 10^6 M_\odot$, which would have gravitationally attracted the surrounding hydrogen/helium gas. Whether or not the gas in the halo collapses is subsequently determined mainly by the Jeans mass, which depends on temperature and particle density (Bromm et al. 2009). The first numerical simulations in the early 2000's sought to offer an estimate of the individual stellar mass of stars forming in these regions. Bromm et al. (1999), Nakamura & Umemura (2001) and Abel et al. (2002) were some of the pioneering groups seeking a clue to the ever important question regarding the IMF of Pop III stars. Their simulations centred on investigating how the collapsing gas cloud would fragment during the process. The degree of fragmentation would then play an important role in the individual mass of Pop III stars. These, and other simulations, hinted at very massive Pop III stars, generally with a stellar mass higher than $100 M_\odot$. Later simulations, such as those done by O'Shea & Norman (2007) using similar methods, showed a broader range of possible masses but also a lower minimum mass – $30 - 300 M_\odot$. A stellar IMF where most of the stars are (very) massive and in the range of $\sim 100 M_\odot$ is often considered to be (extremely) 'top-heavy', and is referred to as Pop III.1 (see section 1.1.1).

More recent simulations taking into account factors such as accretion and evaporation of the protostellar disks that form after collapse and fragmentation, puts an upper limit of the Pop III IMF at $\sim 40 M_\odot$ (Hosokawa et al. 2011). In addition to simulations on star formation, there are other approaches in determining the Pop III IMF. Joggerst et al. (2010) found in their work that core-collapse supernovae from $15 - 40 M_\odot$ Pop III stars would have been enough to contribute most of the metals to the early Universe. A stellar IMF in this range is generally referred to as Pop III.2 and is believed to be top-heavy, something which will be explored in more detail in the next section.

1.1.1 The Pop III stellar IMF

To start with, it might be a good idea to clarify the nomenclature used for the various Pop III IMF models. The naming convention that is most commonly used, is the following (Greif et al. 2010).

Pop III.1: Considered the true 'first generation' stars of primordial composition (i.e. elements produced by Big Bang nucleosynthesis), and are considered to have formed only through the influence of the initial cosmological conditions, i.e. as described in a simplified manner, at the start of section 1.1.

Pop III.2: This would be the 'second generation' of Pop III stars, still sharing the same primordial composition as Pop III.1. Unlike Pop III.1,

these stars are thought to have formed under the influence of feedback mechanics, e.g. radiative effects which would have heated and ionized the gas from which Pop III.2 stars then formed.

In addition to these two, this work uses another Pop III model based on the normal stellar IMF, often referred to as the universal Kroupa (2001) IMF, which originates in the works of Pavel Kroupa, e.g. Kroupa (2000) & Kroupa (2001). All the models used in the analysis will be detailed later in section 1.5 – The Yggdrasil population synthesis code.

Since stellar mass is closely tied to the properties of a star, there should be clear differences between the properties of Pop III.1 and Pop III.2 stars. One main difference is how these stars develop as they reach the end of their lives. Pop III.1 stars could be massive enough, $140 - 260M_{\odot}$ assuming no rotation of the star (Chen et al. 2014), to end in *pair instability supernovae* (PISN), which occur when highly energetic gamma rays in the core of the star initiates pair production - electron-positron pairs. As a result of this creation of particles, radiative pressure, which is normally balanced against gravitational contraction, decreases. This then leads to a further contraction of the core which in turn causes the entire core to undergo fusion in a matter of seconds. The energy released due to this sudden and complete fusion of the core essentially destroys the star – disrupts it to a point where no black hole or neutron star remnant is left. If the star has a high degree of stellar rotation, a lower stellar mass limit of $\sim 65M_{\odot}$ is required for a PISN to occur (Chatzopoulos & Wheeler 2012). Such rotation can also cause a star in the $\sim 40 - 65M_{\odot}$ stellar mass range to undergo *pulsational pair instability supernovae* (PPISN), where the pair instability does not result in a complete fusion of the core, but rather causes repeated ejections of shells of matter from the star. As such, a star that experiences a PPISN can continue to evolve, and could at a later stage explode as a Type II supernova, a process which is detailed below.

For the less massive Pop III.2 stars, their fate is also to end in a supernova explosion. These supernovae however are believed to have been of the more common Type II supernovae, also known as a core-collapse supernovae. These occur once fusion of the core is complete, i.e. the core now essentially consists entirely of iron. Since iron is located at a peak when it comes to nuclear binding energy, fusion of iron does not release energy but rather it requires energy to be input into the system. With no more thermal energy from fusion supporting the core against gravitational collapse, a collapse of the star is inevitable. These type of supernovae, while almost as energetic as pair-instability supernovae, do leave a remnant behind, in the form of a neutron star or stellar mass black hole.

This difference in how Pop III.1 and Pop III.2 end their lives might perhaps not seem relevant at first, but the mechanics involved, which I

think are out of the scope of this work, can greatly influence the effect that these supernovae have on the enrichment of the nearby *interstellar medium* (ISM) and the more distant IGM. Today, the current consensus has shifted towards a top-heavy Pop III IMF with a stellar mass of $\sim 40M_{\odot}$ being the most likely. By conducting simulations and comparing with observations, it might be possible to determine which type of supernovae were the dominant ones. In light of this changing consensus, Ritter et al. (2012) investigated how the ISM would be enriched by Type II supernovae, rather than pair-instability supernovae which would be energetic enough to eject a lot of material out of the minihalo into the IGM, rather than just the ISM. They conclude that if Pop III stars had less extreme masses, i.e. more in line with the Pop III.2 IMF, they would enrich the minihalo much faster and as such trigger the formation of Pop II stars earlier. Simulations like these could provide predictions that might be possible to test observationally.

In addition to looking for supernovae, it might also be possible to locate low-mass Pop III stars in the Local Universe. These ideas have come to light in recent years, with the shift towards a lower-mass Pop III.2 IMF. Komiya et al. (2013) investigate the possibility that low-mass Pop III stars, formed as secondary (smaller) companions in binary systems, could have escaped from their minihalos when the primary companion exploded in a supernova, and still exist to this day. They predict that 20-1000 Pop III 'survivors' are located within 2 Mpc of the Milky Way, and might be detectable with coming surveys. Recent simulations conducted by Stacy & Bromm (2014) show that low-mass Pop III stars, $<1M_{\odot} < M \lesssim 5M_{\odot}$, could have formed under unusual conditions and those stars that are around the lower stellar mass limit, are predicted to have survived to this day.

1.1.2 Pop III galaxies

The extensive work of Barkana & Loeb (2001) describes in detail, the formation of the first stars and the hierarchical growth of the CDM halos in which they were formed. The first minihalos of $\sim 10^5 - 10^6 M_{\odot}$ at $z \sim 30$ start to cool down, due to H_2 cooling, and the first stars are formed. However, H_2 is easily dissociated by radiative feedback, so that cooling slows down significantly, and therefore not a lot of the gas in the minihalo will be able to actually form stars (Yoshida et al. 2007). As the hierarchical growth of the minihalos continue, and approach a halo mass of $\sim 10^8 M_{\odot}$ at $z \sim 15$, (see e.g. Fig. 10 in Barkana & Loeb (2001)) cooling by atomic hydrogen becomes efficient enough to allow for greater star formation. Due to the increased mass of these halos, as compared to the first ones that allowed star formation, gas heated by radiative feedback is more easily retained within the halo (e.g. Mori et al. 2002, Kitayama & Yoshida 2005). With these two important effects at work, $\sim 10^8 M_{\odot}$ halos are considered the birthplaces for the first galaxies (Greif et al. 2009).

The nebular gas coverage around these first galaxies plays a very important role, as will be explained further in section 2.3, when trying to use the observed galaxy SED to try to distinguish between different stellar IMFs. Pop III galaxies emit a much stronger Lyman continuum (LyC) at $\lambda < 912 \text{ \AA}$ (i.e. hydrogen-ionizing UV-radiation), compared to regular galaxies that consist of Pop I/II stars. As such, if the SEDs from these strongly LyC emitting galaxies could be compared with Pop I/II SEDs, it might be possible to distinguish them. This is explored at length in the work by Zackrisson et al. (2011), which serves as part of the foundation for this work. They investigate how the SED from a Pop III galaxy changes, if the galaxy is partially or completely covered by photoionized nebular gas. The SED from the radiating gas is essentially obscuring the photometric signature of the Pop III stars, which transforms the appearance of the observed SED into one that looks more like it came from a Pop I/II galaxy. A spectroscopic measurement would still be able to tell the signatures apart, but if the observation is purely photometric as in my case, the signature could be lost. How extensive the nebular coverage is, and thus how big a contribution it makes to the overall SED of the galaxy, is therefore thought to play a large role in determining if it is possible to distinguish a stellar population of Pop III stars from a population of Pop I/II. The effect of this contribution is studied for both WISH and JWST, and is presented alongside the other results in section 2.

1.2 Gravitational lensing

Photons follow the curvature of spacetime, so essentially any massive object such as a star, a galaxy, a cluster or a supercluster of galaxies can act as a gravitational lens, and starlight lensed by the Sun was one of the early validations of general relativity. Today, one widespread use of gravitational lensing is for the purpose of determining the masses of clusters and galaxies, and also the distribution of both regular and dark matter within these objects (e.g. Hoekstra et al. 2013, Oguri et al. 2014). Another example is the diverse field of microlensing, where light from a faint star is amplified by lensing, which was used in e.g. the detection of the lowest-mass brown-dwarf binary system found so far (Choi et al. 2013). Similarly, exoplanets can be detected around stars through microlensing, as the light from a distant background star is lensed by the planet's host star, as the planet transits in front and thus contributes to the lensing effect.

The most important property of lensing when it comes to the search for Pop III galaxies, is the very high levels of magnification (μ) that can be obtained. Just like a regular lens can magnify an object, a gravitational lens can, under the right conditions, magnify/boost the flux of an object like a galaxy up to 100 times, i.e. $\mu = 100$ (Zackrisson et al. 2012). Smaller objects like a quasar or a Pop III galaxy, could be magnified even further.

This comes naturally as a result of the lensing effect, since the area in the source plane subject to such powerful lensing becomes smaller, the greater the magnification is. As a result, you might be able to obtain an extreme magnification ($\mu > 100$) of a cluster of Pop III stars, but not of the surrounding nebula. To illustrate the effect of lensing, Fig. 1 depicts four lensed and highly magnified images of a quasar as well as a fifth, weaker lensed image of the quasar, and a triply lensed galaxy (Sharon et al. 2005).

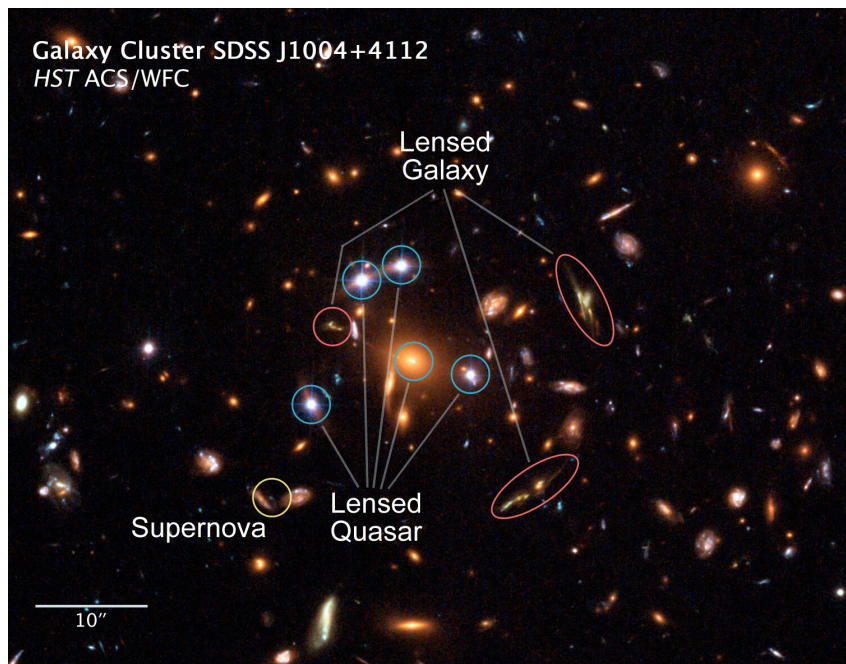


Figure 1: Example of a multiply lensed object (strong gravitational lensing). Originally identified by Sharon et al. (2005) using observational data from HST. Image obtained from NASA, ESA 2006 Release #: [STScI-2006-23](#)

Zackrisson et al. (2012) investigate the possibility of detecting gravitationally lensed Pop III galaxies using HST and JWST, relying on a boost to the flux of the Pop III galaxies by $\mu \sim 100$. I will be focusing mostly on a redshift of $z = 8.5$, for reasons that will be explained in section 2.1, and as seen in Fig. 2 they predict ~ 100 Pop III galaxies per arcmin² at this redshift.

Recent research into this field has posited that $\mu > 100$ could be attainable for small objects such as a Pop III galaxy (Zackrisson et al. 2014, in prep). The probability of finding such an extremely lensed object would depend on the desired magnification, as indicated by Fig. 3, but overall the probability is rather low. There will be little to no chance for say, JWST to locate one of these since it focuses on a small piece of the sky at a time. WISH on the other hand will, as part of its primary mission, perform an

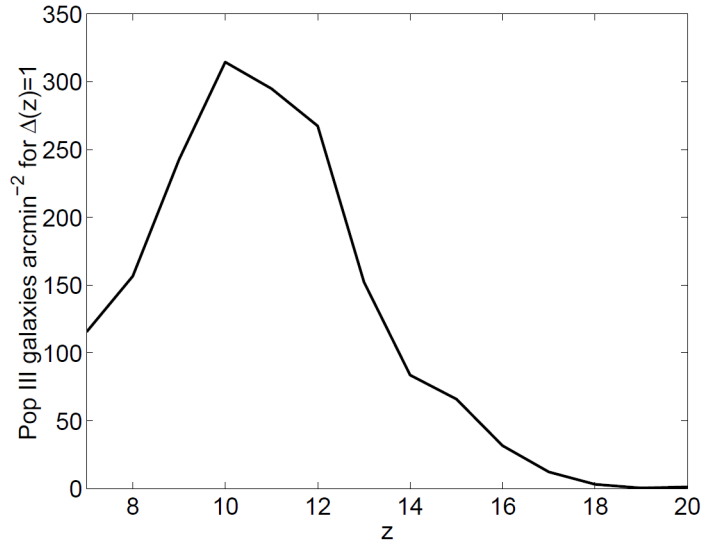


Figure 2: Population density of Pop III galaxies as a function of redshift (Zackrisson et al. 2012).

Ultra Deep Survey (UDS) covering 100 deg^2 , which, given the above estimate, would mean $\sim 3.6 \times 10^7$ Pop III galaxies. Given this large survey area, WISH could hopefully locate Pop III galaxies boosted to such an extent, by gravitational lensing with $\mu > 100$, that they fall within its detection limits, and I will discuss this more at the end in section 3.

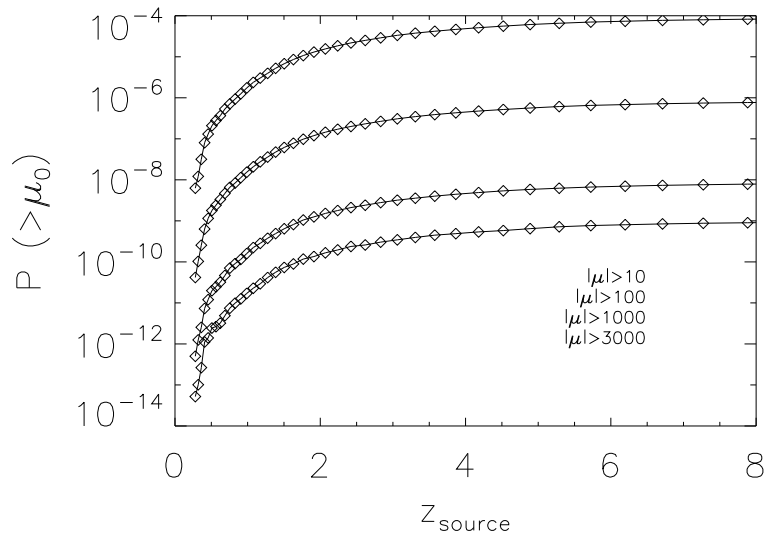


Figure 3: Probability of finding sources with extreme magnification as a function of redshift (Zackrisson et al. 2014, in prep).

1.3 The WISH mission

Detailed observations done in the infrared (IR) are best performed in space, since the Earth's atmosphere absorbs a great deal of IR-radiation and as with all ground based telescopes, the atmosphere also causes blurring and a loss of detail. For this reason, the most capable IR telescopes are, naturally, space based telescopes. This of course puts extensive restrictions on their size, construction and maintenance, and also leads to a substantial increase in cost and planning time.

The planned 1.5 m WISH telescope, and its wide-field *near infrared* (NIR; $\lambda \approx 1 - 5\mu\text{m}$) camera with a Field of View of ~ 850 arcmin², is part of a primarily Japanese mission specifically designed for detecting the very first galaxies in the early Universe, $z > 7$. Other goals of the mission include furthering the understanding of re-ionization, and broader studies of later galaxy formation and evolution at $z < 7$. It is uniquely suited to many of these tasks, given the very wide-area sky surveys that would be made possible by its NIR camera. Since the mission is still in the proposal stage, it could be prone to change and the details presented here are based on the WISH Sensitivity and Survey Plan¹, presented at the latest WISH international workshop in December 2013 by Kiyoto Yabe. Seven different broad band filters are planned, in the $1.0\mu\text{m} - 4.5\mu\text{m}$ range, the first five of which can reach a sensitivity of 28 AB magnitudes, at a *signal to noise ratio* (S/N) of 3σ in 10-20h. These five filters – $1.040\mu\text{m}$, $1.360\mu\text{m}$, $1.775\mu\text{m}$, $2.320\mu\text{m}$ and $3.030\mu\text{m}$ – are used in the UDS and are also the ones used for the Yggdrasil code, and therefore the ones I have examined. The UDS is estimated to take about 4 years, out of a planned mission length of five years, to be completed at 28.0 mag (3σ). An even deeper survey to attain higher sensitivity would be possible, but only for the first three filters and a substantially increased survey time. Covering the same area in the sky at 28.5 mag (3σ) would take an additional ~ 4 years, and going to 29.0 mag (3σ) would require ~ 8 more, for a total of ~ 16 years. As such, it seems more realistic to assume a limiting sensitivity of 28.0 mag (3σ) for the purposes of this work.

1.4 The James Webb Space Telescope

The JWST is a much larger, and much delayed, project lead by NASA with significant contributions from ESA and others, currently planned to launch in 2018. The primary mirror will be about four times larger compared to WISH, with a diameter of ~ 6.5 m, and the telescope will carry four different scientific instruments. The primary mission of JWST is expected to last 5-10 years and among the main mission goals is the search for the first galaxies, studying galaxy evolution, observing stars in the early stages

¹http://wishmission.org/files/20131202/dec2/03-kiyoto_yabe.pdf

of forming planetary systems, measuring the properties of such systems and investigating the potential for life therein.

Since the JWST project has a scope much greater than that of WISH, I will only discuss the instrument relevant to this work, the *Near Infrared Camera* (NIRCam)², but also mention the *Near Infrared Spectrometer* (NIRSpec) which could be used to do follow-up spectroscopical measurements. The wavelength range of NIRCam is $0.6\mu m - 5.0\mu m$ and the instrument divides that range into two channels ('short': $0.6\mu m - 2.3\mu m$ and 'long': $2.4\mu m - 5.0\mu m$). Unlike the (very) wide-field camera on WISH, NIRCam has a very narrow Field of View and is meant to really 'zoom in' on an area and do a detailed survey. It does this through the use of two modules, each with a Field of View of 2.16×2.16 arcmin², and since either module can operate in the short or long band, it is possible to observe in two different filters at once. The filters available to me, via Yggdrasil, are F070W ($0.7\mu m$), F115W, F150W, F200W, F277W, F356W and F444W, but for reasons discussed in section 2.2 I primarily make use of four filters, F150W to F356W.

To hunt for Pop III galaxies, one would ideally want to use two telescopes such as these. One, like WISH, is specialized in wide-field surveys that cover a large part of the sky, and thus a great many candidate galaxies, while the other, such as JWST, is specialized in doing a much more deeper and detailed survey of a potential Pop III galaxy candidate. The 'problem' with WISH is that it will not really be possible to increase the exposure time in the UDS, and thus not increase S/N above 3σ . With such a low S/N, you run the risk of being unable to say anything concrete about what you actually observe (photometrically). JWST on the other hand, allows for observations with a variable exposure time, and can therefore reach significantly higher S/N with relative ease. Using them in combination allows you to locate potential candidates with WISH, and thereafter do more detailed surveys with JWST to determine if what you have found could actually be a Pop III galaxy. Finding the right balance between exposure time and higher precision will likely be a tricky prospect – allocate too much time on the one object and you potentially neglect many others. This will be explored further in the latter part of the Results section.

1.5 The Yggdrasil population synthesis code

Yggdrasil³ was developed by Zackrisson et al. (2011) for modelling and predicting the SEDs, and magnitudes, of mainly high redshift galaxies, using various IMFs and metallicities ($Z \geq 0$). It is capable of presenting the data using filters from a number of current and upcoming telescopes, including

²<http://www.stsci.edu/jwst/instruments/nircam/>

³Accessible to me at: <http://ttt.astro.su.se/projects/yggdrasil/yggdrasil.html>

WISH and JWST/NIRCam. In addition to offering many IMF and metallicity combinations, it also provides options for including nebular gas coverage ($f_{cov} = 0.0, 0.5, 1.0$) and subsequent contribution to the SED, variable burst SFR – instant burst or initial burst with continuous SFR for 10, 30 or 100 Myr – and the last input parameter, Lyman- α transmission factor, was set to 0. The SFR chosen was one with an initial burst followed by a constant SFR for 10 Myr, after which the SFR immediately drops to zero. When it comes to gas coverage factors, I start out with $f_{cov} = 0$ and later use models with $f_{cov} = 1.0$ to determine at which percentage of nebular coverage the ability to distinguish between Pop III, Pop I/II and EMP stellar models is lost. In regards to redshift, the data I work with contain data representing a full range coverage of $0 \leq z < 15$, in increments of 0.25. However, as will be detailed in section 2.1, I end up using only a small part of this interval, following the data selection process. The thirteen stellar models provided by Yggdrasil and included in this work are

- Pop III.1, featuring an extremely top-heavy IMF, $50 - 500M_{\odot}$ and using a *single stellar population* (SSP) from Schaerer (2002).
- Pop III.2, featuring a moderately top-heavy IMF in a stellar mass interval of $1 - 500M_{\odot}$ with a characteristic mass of $10M_{\odot}$, with an SSP from Raiter et al. (2010).
- Pop III Kroupa, which uses the universal Kroupa (2001) IMF and stellar masses of $0.1 - 100M_{\odot}$, based on a rescaled SSP from Schaerer (2002).
- Four different Pop I/II models with metallicities $Z = 0.0004, 0.004, 0.008, 0.020$, all using the universal Kroupa (2001) IMF and stellar masses of $0.1 - 100M_{\odot}$ and based on a Starburst99 SSP from Leitherer et al. (1999), Vazquez & Leitherer (2005).
- Six EMP models (WISH only) with metallicities $Z = 10^{-5}$ and $Z = 10^{-7}$. For each metallicity, a model was constructed using the Pop III.1, Pop III.2 and the universal Kroupa (2001) IMFs listed above.

Data from Yggdrasil is provided in lists, containing columns for redshift, stellar age, stellar population mass, and then AB magnitudes in the relevant filters for WISH or JWST/NIRCam. The magnitude output from Yggdrasil is adjusted to the stellar population mass, which in my case means either $1M_{\odot}$ or 10^6M_{\odot} . Adjustments can be made to the magnitude data, to roughly determine which combination of stellar population mass and magnification would be required for the magnitudes to come within the detection threshold of 28 mag for WISH.

An adjustment to the magnitude, due to a higher/lower stellar population mass is applied using

$$\Delta m_{mass} = -2.5 \log_{10} \left(\frac{M_1}{M_2} \right) \quad (1)$$

where M_2 would be the stellar population mass used by Yggdrasil, and M_1 the stellar population mass one wants to adjust to. Similarly, a boost to the magnitude through magnification is added as

$$\Delta m_{lens} = -2.5 \log_{10}(\mu) \quad (2)$$

One possible combination of these parameters, that could allow detection by WISH and JWST, is a stellar population mass of $6 \times 10^4 M_\odot$ and a magnification of $\mu = 1000$. This will be discussed further in section 3.

So with the models at hand, the main idea behind the method is simple. Using the different filters for either telescope, one can create a 'colour' combination by subtracting the magnitude of a model in one filter at a specific redshift, from a filter with a shorter wavelength at the same redshift, e.g.

$$\Delta m = m_{1.360\mu m} - m_{2.320\mu m} \text{ for WISH, and}$$

$$\Delta m = m_{F150W} - m_{F277W} \text{ for JWST/NIRCam.}$$

By doing this for models with different IMFs and then plotting their respective magnitude data using a colour combination, it is possible to distinguish between the models by looking at the 'blueness' of a model (essentially the slope of the continuum, in the absence of emission lines). The Yggdrasil data can be processed in e.g. Python (see Appendix for a code sample), and presented like in Fig 4 & 5, where the zero metallicity Pop III IMFs can be seen to be clearly separated from the Pop I/II models.

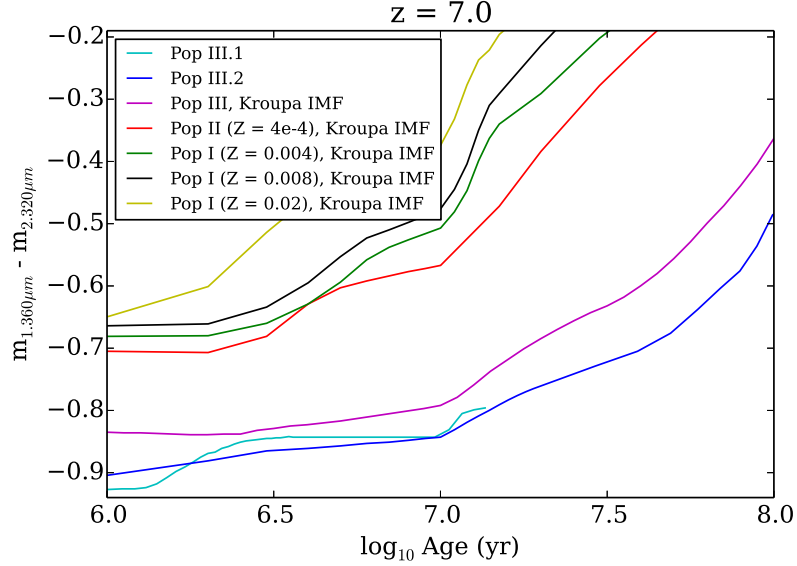


Figure 4: A colour combination of the second and fourth filters used in the WISH UDS, modelled at $z = 7$. Note how the last Pop III.1 stars die off shortly after ~ 10 Myr, the cut off for the constant SFR, due to their exceedingly short lifespans. All other models become increasingly 'redder' with age, as massive stars die off and lower-mass stars evolve.

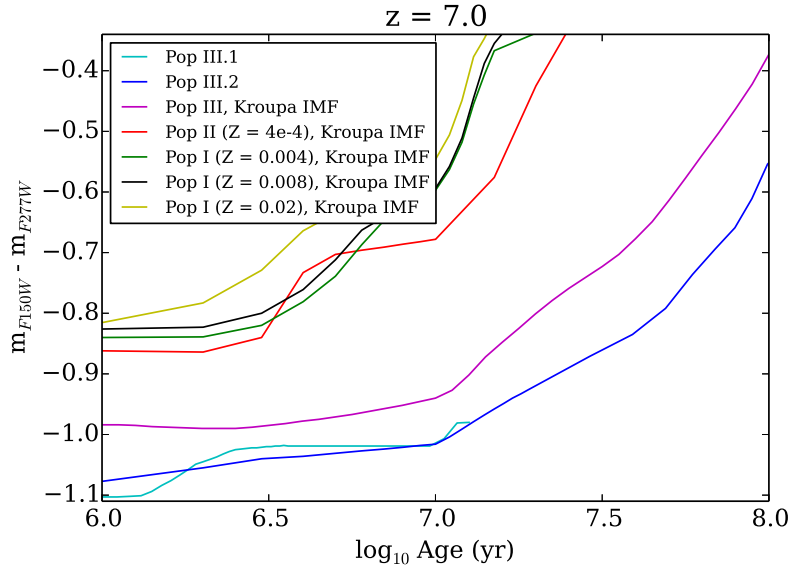


Figure 5: The equivalent colour combination for JWST/NIRCam, at slightly different wavelengths, modelled at $z = 7$.

2 Results

In this section I intend to first present the process of data selection according to several criteria. Following that, the results and conclusions I have reached regarding the prospect of future detection of Pop III galaxies using WISH and JWST/NIRCam, will be presented.

2.1 Selecting the optimal redshift and filter combination

Other than my own criteria that I have set up, there is one specific problem that puts a hard limit on which filters I can use at which redshift – the Lyman break at 1216 Å.

Before discussing that however, one additional factor that is worth considering for selecting an appropriate redshift, is the population density of Pop III galaxies you might expect to find at various redshifts. As previously shown in Fig. 2, there is a sharp decline in the number of expected Pop III galaxies at $z \lesssim 8.5$, so if a filter combination performs equally well at $z = 7.0$ as $z = 8.5$ it seems reasonable to focus on the higher redshift.

2.1.1 Lyman break at 1216 Å limits filter selection

The classical Lyman break refers to the absorption of $\lambda < 912$ Å photons by the ISM. There is however a second break that occurs at higher redshifts at $\lambda = 1216$ Å (i.e. at the Lyman- α rest frame emission line), which effectively limits the usefulness of some of the available filters past a certain redshift. This Lyman- α break, also known as the Gunn-Peterson trough, is also caused by the absorption of photons by neutral hydrogen, but this time in the IGM. This gives rise to the term "Lyman- α forest", that refers to the repeated absorption of photons over long distances that yields hundreds of absorption lines when viewed spectrographically. The 1216 Å break was first predicted by Gunn & Peterson (1965) and later detailed extensively by Madau (1995), but has also been updated recently, e.g. Inoue et al. (2014), and Fig. 4 in their work illustrates the effect the break has on Lyman- α transmission at $z < 6$.

This Lyman break makes it impossible to use a colour combination created from two filters, where one suffers from high Lyman- α transmission, since the colour would become far redder than it otherwise would be. Fortunately, by using the information contained in the transmission files for WISH and JWST/NIRCam used in Yggdrasil, which lists the Lyman- α transmission profiles and observed wavelengths at the start of the break, it is possible to estimate the redshift at which a filter is unsuitable for photometric use in this work. If the acceptable amount of transmission is deemed to be < 0.05 and eq. (3) is used, the following values in Table 1 are obtained.

$$z = \frac{\lambda_{obs} - \lambda_{em}}{\lambda_{em}} \Leftrightarrow \lambda_{obs} = \lambda_{em}(1 + z) \quad (3)$$

Table 1: Wavelengths and redshifts after which the break interferes significantly with photometric measurements. Filters operating at wavelengths longer than these are not affected in the redshifts that are relevant for this work.

WISH	λ_{break} [μm]	z_{break}	JWST	λ_{break} [μm]	z_{break}
1.040 μm	0.880	6.23	F070W	0.606	3.98
1.360 μm	1.164	8.57	F115W	0.998	7.21
1.775 μm	1.520	11.50	F150W	1.316	9.82
			F200W	1.754	13.42

As can be seen from Table 1 above, the JWST/NIRCam F070W filter is only photometrically reliable up to $z \sim 4$, where it starts to experience a decrease in flux, which continues until it reaches zero around $z \sim 6.25$. For this reason it was never considered as a valid option. The WISH 1.040 μm filter suffers from the same problem, with it being limited to too low redshifts to be worth considering, since it starts to experience a loss of flux around $z \sim 6.2$, reaching zero at $z \sim 8.5$. F115W has similar problems with being limited to $z < 7.2$, and is therefore excluded at higher redshifts. Likewise, 1.360 μm is limited to $z < 8.5$.

We thus arrive at the final filter selection of 1.360 μm , 1.775 μm , 2.320 μm and 3.030 μm for WISH, as well as F150W, F200W, F277W and F356W for JWST/NIRCam. These are then used to create the three colour combinations used for the analysis, and we move on to the next two criteria.

2.1.2 Filter performance depends on redshift

In addition to the limits put in place by the Lyman break at 1216 Å, there are two criteria that influences the selection of the final filter and redshift combination. Of these two, the primary criterion is the fact that the filter colour performance, i.e. obtaining the largest separation between models, varies with redshift. Fig. 6 uses the same colour combination as seen in Fig. 4, but this time shown at $z = 8.5$. The maximum separation, Δm_{max} , between Pop I/II and Pop III models increases significantly, and if used at redshifts $z < 7$, the separation decreases. The same trend is observed for other WISH colour combinations using the same range of filters, e.g. $m_{1.360\mu m} - m_{1.775\mu m}$, $m_{1.360\mu m} - m_{3.030\mu m}$.

Beyond $z = 8.5$, a different colour would be needed, e.g. $m_{1.775\mu m} - m_{3.030\mu m}$, shown in Fig. 7 at $z = 8.5$ and Fig. 8 at $z = 11.5$. Note the large difference in Δm_{max} between the models, in Fig. 6 & 7. This illustrates the importance of selecting the right filter combinations for a specific redshift. Obtaining a Δm_{max} for $m_{1.775\mu m} - m_{3.030\mu m}$ that is equivalent to $m_{1.360\mu m} - m_{2.320\mu m}$ at $z = 8.5$, a redshift of $z \sim 11.5$ is required (Fig. 8).

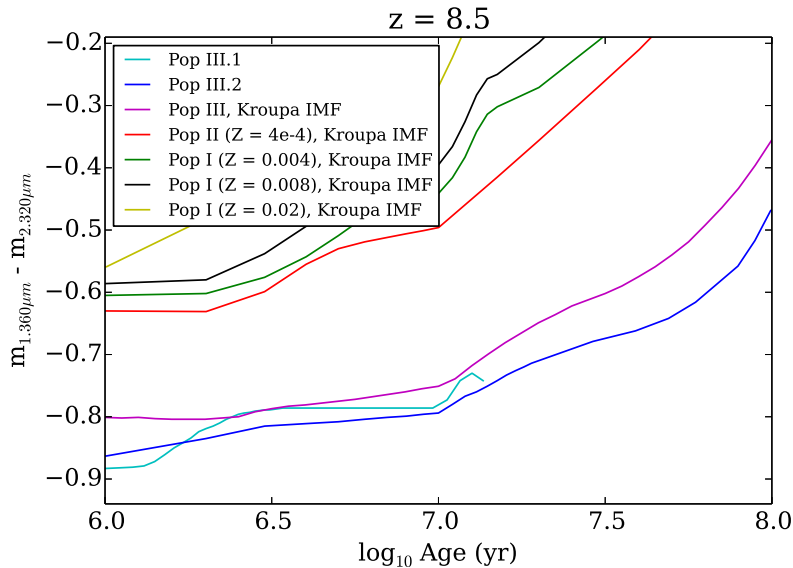


Figure 6: The WISH $m_{1.360\mu m} - m_{2.320\mu m}$ colour shown at $z = 8.5$. Compared with Fig. 4 at $z = 7.0$, Δm_{max} between Pop I/II and Pop III models increases by $\sim 15 - 30\%$.

While perhaps not entirely unexpected, since the filter has picked as many rest-frame UV photons as it is able to, the maximum separation between the models is obtained just before the break sets in. The same behaviour can be seen with JWST/NIRCam colours but at slightly different redshifts, since F150W encounters the break at $z \sim 9.8$. As such, colours using F150W as the first filter will be slightly weaker at $z = 8.5$, but not by such a drastic difference as seen between Fig. 6 & 7.

Since both telescopes need to be used in cooperation, i.e. observe at the same redshift, I feel $z = 8.5$ is the best option. It is of course possible to go to higher redshifts around $z \sim 11$, but a similar problem would occur yet again when using F200W as the first filter.

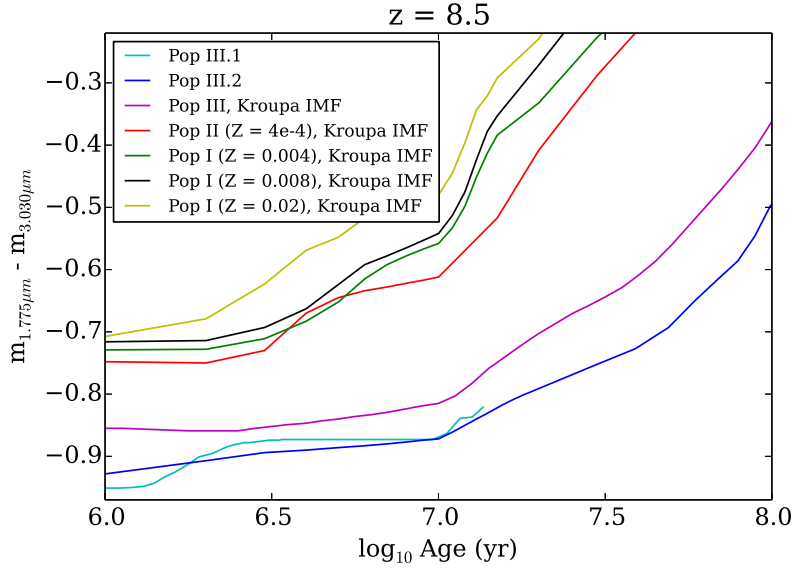


Figure 7: The WISH $m_{1.775\mu m} - m_{3.030\mu m}$ colour shown at $z = 8.5$. Δm_{max} is $\sim 30\%$ smaller compared to $m_{1.360\mu m} - m_{2.320\mu m}$ at the same redshift, as seen in Fig. 6.

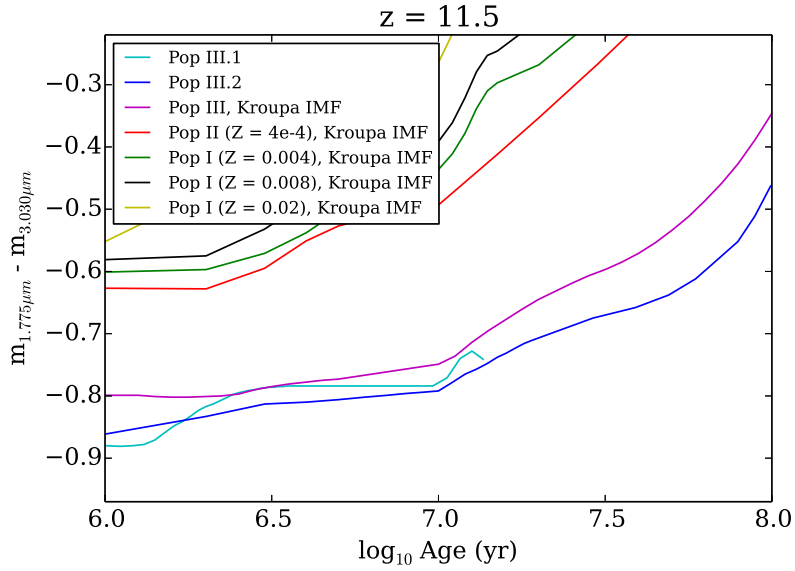


Figure 8: The WISH $m_{1.775\mu m} - m_{3.030\mu m}$ colour shown at $z = 11.5$. Δm_{max} is similar when compared with Fig. 6

2.1.3 Finding the optimal filter combination

Thus far, only the second colour combination, i.e. filter 1 - filter 3, e.g. $m_{1.360\mu m} - m_{2.320\mu m}$, has been used in the plots, and the reasoning behind this choice will now be explained.

A slightly more subtle criterion involves how Δm_{max} changes with different colours. For the colours used here, it generally followed that the greater the wavelength separation between two filters used for a colour, the greater the maximum possible separation between Pop I/II and Pop III models. This is illustrated at $z = 8.5$ with the JWST/NIRCam colours $m_{F150W} - m_{F200W}$, $m_{F150W} - m_{F277W}$ and $m_{F150W} - m_{F356W}$, in Fig. 9, 10 and 11.

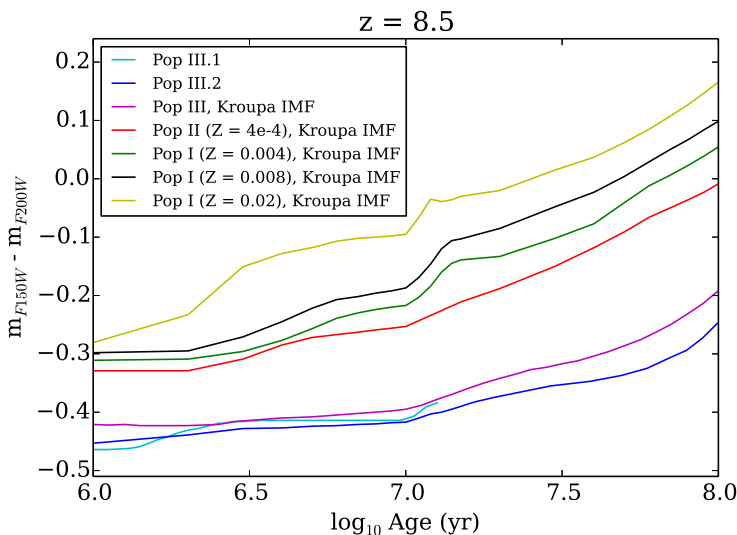


Figure 9: The JWST/NIRCam $m_{F150W} - m_{F200W}$ colour shown at $z = 8.5$. This first colour combination has the shortest difference in wavelength, $0.5\mu m$. The equivalent for WISH is $0.415\mu m$ for the $m_{1.360\mu m} - m_{2.320\mu m}$ colour.

Comparing Fig. 10 and Fig. 11, it is evident that the latter shows a greater separation between Pop I/II and Pop III models, so why has this not been the colour combination of choice so far?

The main reason pertains to the addition of nebular flux contribution to the models, detailed in the next section. Essentially, it turned out that the third colour combination was extremely sensitive to this nebular contribution, and the Pop III models 'reddened' much faster compared to the first or second colour combination. As a result, the benefit of the greater separation observed in Fig. 11 at 0% nebular contribution, is very rapidly lost when any of this contribution is factored into it.

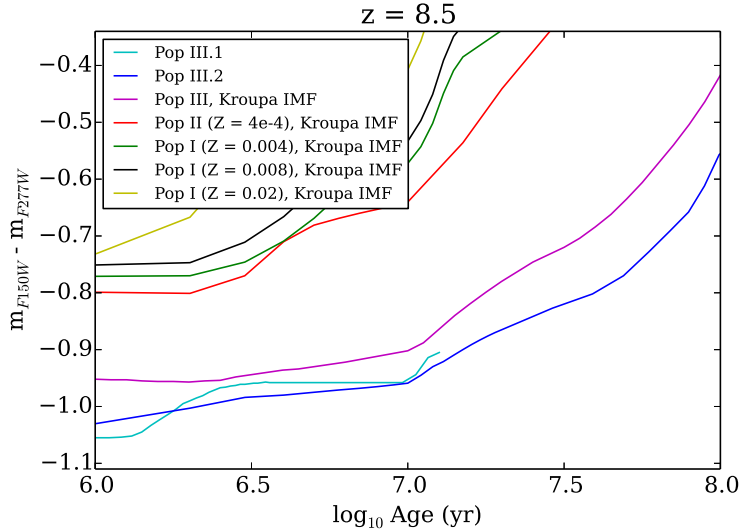


Figure 10: The second JWST/NIRCam colour combination, $m_{F150W} - m_{F277W}$, shown at $z = 8.5$. Δm_{max} between Pop I/II and Pop III models is roughly equal to when compared with the WISH $m_{1.360\mu m} - m_{2.320\mu m}$ colour in Fig. 6.

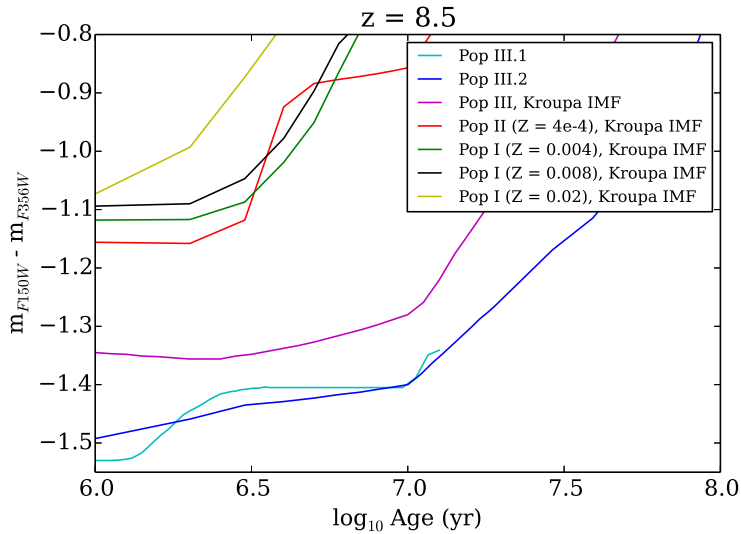


Figure 11: The third and final JWST/NIRCam colour combination, $m_{F150W} - m_{F356W}$, shown at $z = 8.5$.

While the first colour combination is less sensitive to nebular contribution, the initial separation is also significantly lower as can be seen in Fig. 9 – about half that of the second colour combination in Fig. 10. The above reasoning applies equally to the WISH filters, and therefore we end up with

the second colour combination being the preferred one – e.g. Fig. 18.

2.2 Adding nebular gas cloud emissions

As was discussed in section 1.1, the SED from photoionized nebular gas is expected to play an important role in potential photometric measurements of Pop III galaxies. How big of an influence the nebular gas around the stars in these galaxies has, depends on the nebular coverage factor (f_{cov}), which essentially describes how large a fraction of ionizing radiation from the stellar sources is absorbed and re-emitted by surrounding gas.

In their work, Zackrisson et al. (2011) consider three models of nebular coverage of Pop III galaxies. In the first one, *type A*, the galaxy is for all intents and purposes completely covered and very little ionizing radiation escapes – since the SED is dominated by nebular emission – and this would be represented in Yggdrasil by $f_{cov} = 1.0$. At the other extreme, *type C*, the nebular gas has been pushed out far enough that it no longer contributes to the overall SED, which is essentially what I have assumed so far by using Yggdrasil models with $f_{cov} = 0$. In between lies a hard to predict combination, *type B*, where there is a partial nebular coverage and contribution to the SED.

Since it seems unlikely that one would find Pop III galaxies completely devoid of any nebular contribution to the overall SED, investigating which fraction of f_{cov} still allows for a distinction to be made between Pop I/II and Pop III SEDs is crucial.

To achieve this, data for all the models, except the EMP models⁴, was generated again using Yggdrasil, this time assuming full nebular coverage, i.e. $f_{cov} = 1.0$. To obtain the nebular contribution for any given model, the magnitude data in both the $f_{cov} = 0$ and $f_{cov} = 1.0$ models was first converted to flux, using eq. (4). Then, assuming a linear relation for the flux contribution from the nebular gas, the flux of the $f_{cov} = 0$ model was subtracted from the $f_{cov} = 1.0$ model, leaving a model with only the nebular component. Fractions of this nebular component was then added to flux data in the original $f_{cov} = 0$ model, and the total flux was then converted back into magnitudes. In the end, this method allows for a given fraction of f_{cov} to be easily added onto the base model with $f_{cov} = 0$, to simulate an incremental nebular contributions.

$$m = -2.5\log_{10}(F) \Leftrightarrow F = 10^{-\frac{m}{2.5}} \quad (4)$$

Fig. 12, 13 & 14 illustrate what effect a contribution of $f_{cov} = 0.05$, for all models, has on the three different colour combinations in the JWST/NIRCam system. As mentioned previously, both the models and the

⁴All the EMP models were provided by my supervisor, Erik Zackrisson, as they were not available to me via the access I had to Yggdrasil.

colours all react differently to increasing nebular contribution. Fig. 15, $m_{F150W} - m_{F200W}$ at $f_{cov} = 0.20$, illustrates the futile situation one ends up with, if the nebular contribution to the overall Pop III galaxy SED is more than a few percent. As will also be shown in section 2.4, the fraction of f_{cov} added to the Pop III galaxy SED that can be tolerated is even lower if EMP models ($f_{cov} = 0$) are included in the analysis.

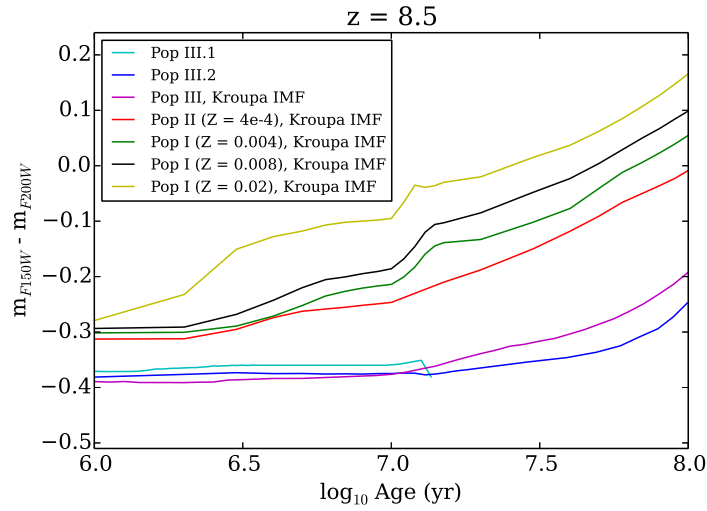


Figure 12: The JWST/NIRCam $m_{F150W} - m_{F200W}$ colour with $f_{cov} = 0.05$ (all models). Compare with Fig. 9 for the overall effect of added nebular contribution.

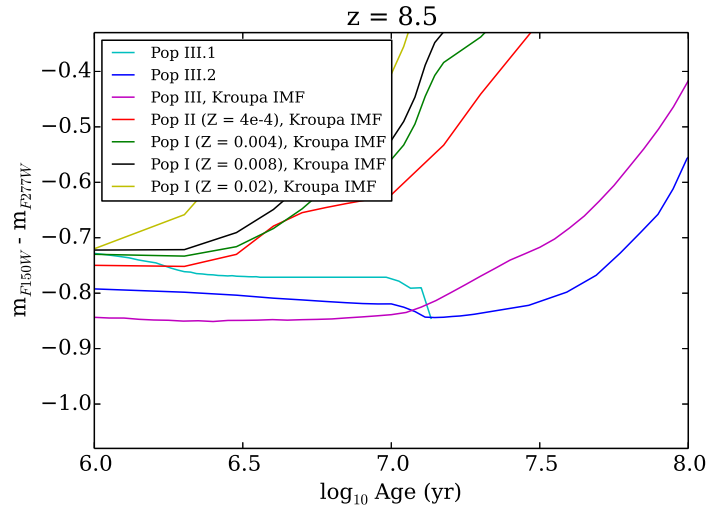


Figure 13: The JWST/NIRCam $m_{F150W} - m_{F277W}$ colour with $f_{cov} = 0.05$ (all models). As before, compare with Fig. 10.

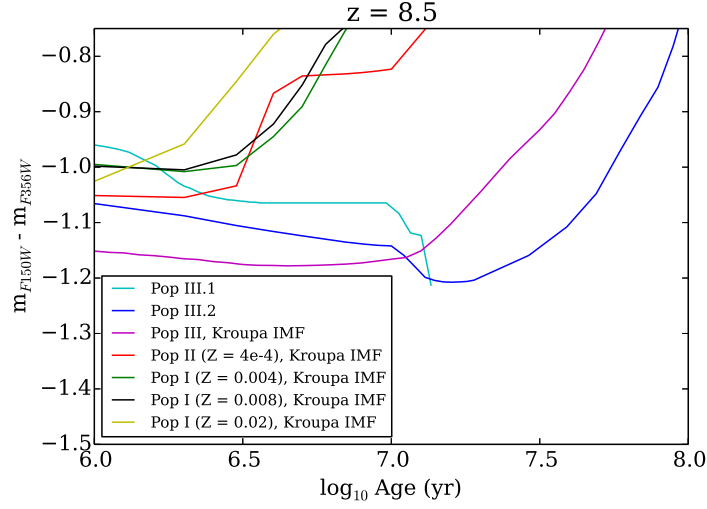


Figure 14: The JWST/NIRCam $m_{F150W} - m_{F356W}$ colour with $f_{cov} = 0.05$ (all models) clearly illustrates the much more rapid reddening of the Pop III models, compared to the other colour combinations. Again, also compare with Fig. 11.

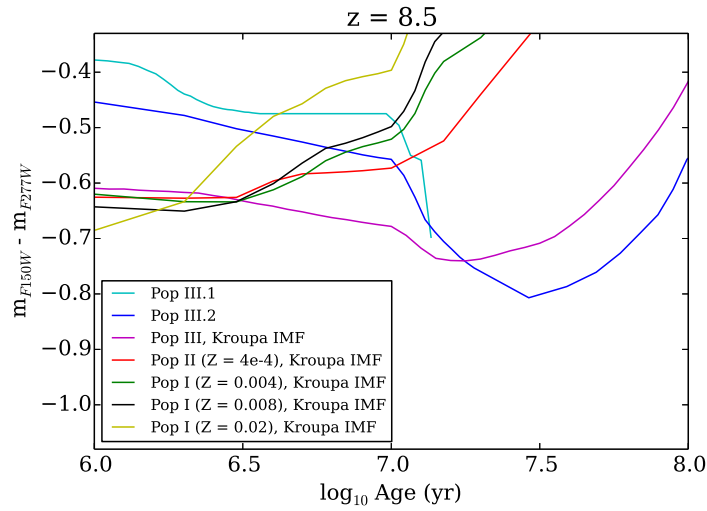


Figure 15: The JWST/NIRCam $m_{F150W} - m_{F277W}$ colour with $f_{cov} = 0.20$. It is evident that anything more than a few percent completely invalidates any photometric distinction.

2.3 Including EMP galaxy models for WISH

So far, all Pop III IMFs have seemed to be reasonably well separated from Pop I/II models, given no nebular contribution. However, it is possible that there are small galaxies dominated by EMP stars, which, depending on their IMFs, could end up with photometric signatures very similar to Pop III galaxies. Therefore, the six different WISH EMP models previously detailed were included and examined.

How well they blend in with Pop III models was investigated using the WISH filters, first without and later with nebular contribution taken into consideration. Examples of the former are presented in this section as Fig. 16 & 17. As might be expected, both EMP models using the Kroupa IMF are far bluer than the $Z = 0.0004$ Pop II model, and the lowest metallicity EMP Kroupa IMF model ends up very close to the Pop III Kroupa IMF model.

Pop III.2 is currently considered to be the best candidate for representing the typical IMF in a Pop III galaxy, and Fig. 17 perfectly illustrates the major complications that EMP galaxies could give rise to, when trying to distinguish the Pop III IMF. Even assuming no nebular contribution, it is clear that EMP galaxies could severely hamper such efforts, and just how much, if any, nebular contribution can be tolerated, will be looked at next.

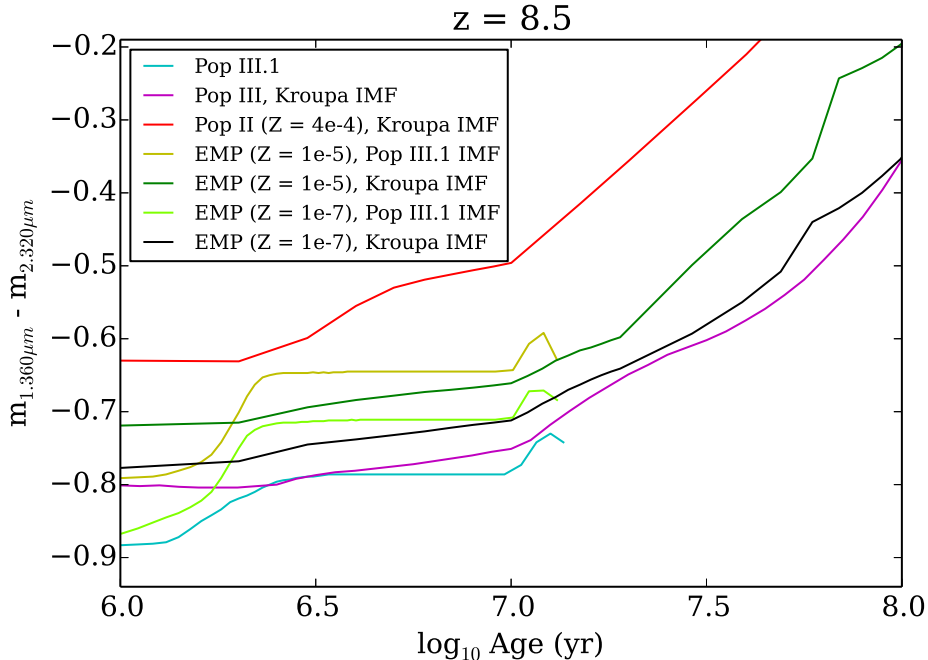


Figure 16: EMP models using the Kroupa and Pop III.1 IMFs and their Pop III counterparts, shown in the WISH $m_{1.360\mu m} - m_{2.320\mu m}$ colour with $f_{cov} = 0$.

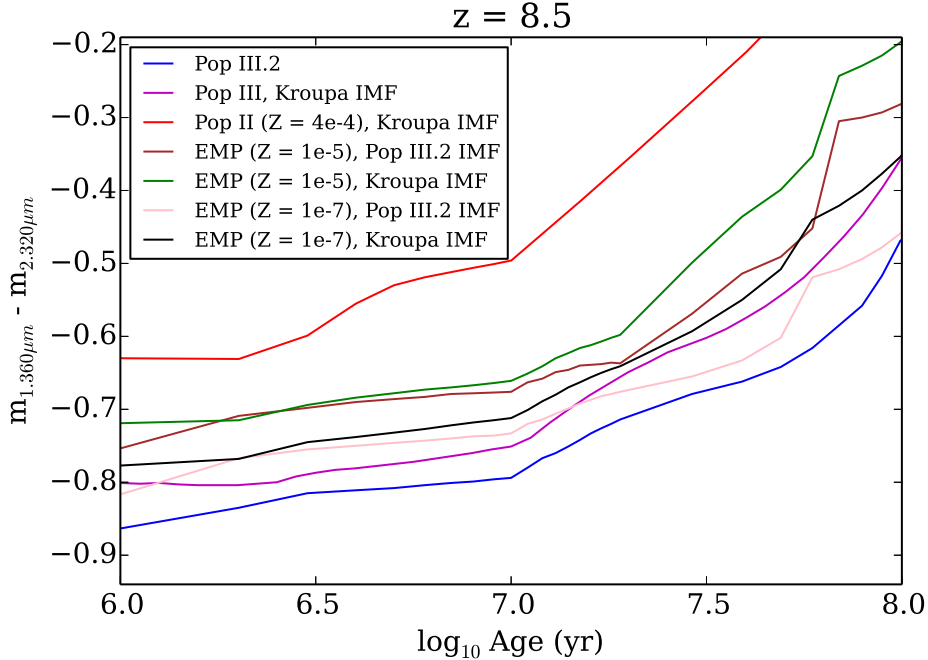


Figure 17: EMP models using the Kroupa and Pop III.2 IMFs and their Pop III counterparts, shown in the WISH $m_{1.360\mu m} - m_{2.320\mu m}$ colour with $f_{cov} = 0$.

2.4 Final WISH results

While this method of distinguishing the Pop III IMF from others shows promise, there are, as I have shown, several things that need to be taken into serious consideration, other than just the choice of redshift or filter combinations. Nebular contribution to the Pop III SED makes it appear redder, while EMP galaxies in turn narrow Δm_{max} significantly. If the EMP IMF is very similar to Pop III.2, it should prove enormously difficult to distinguish the two photometrically, even at $f_{cov} = 0$ as seen in Fig. 17 above. But if they have an IMF very similar to Pop I/II stars, there is still a chance we might be able to tell them apart, with a fractional f_{cov} contribution.

Assuming the 'worst case scenario' where EMP galaxies have a pure stellar SED, and a Pop III galaxy has a SED with both stellar and nebular components, which fraction of f_{cov} can be applied before the signature of the Pop III IMF is lost? Fig. 18 could be viewed as the final result of this work, considering all that is factored into its analysis. In this worst case scenario, the margins are quite slim and only $\sim 1\%$ of nebular emission (dashed lines) contributing to the overall SED can be reasonably tolerated by this method.

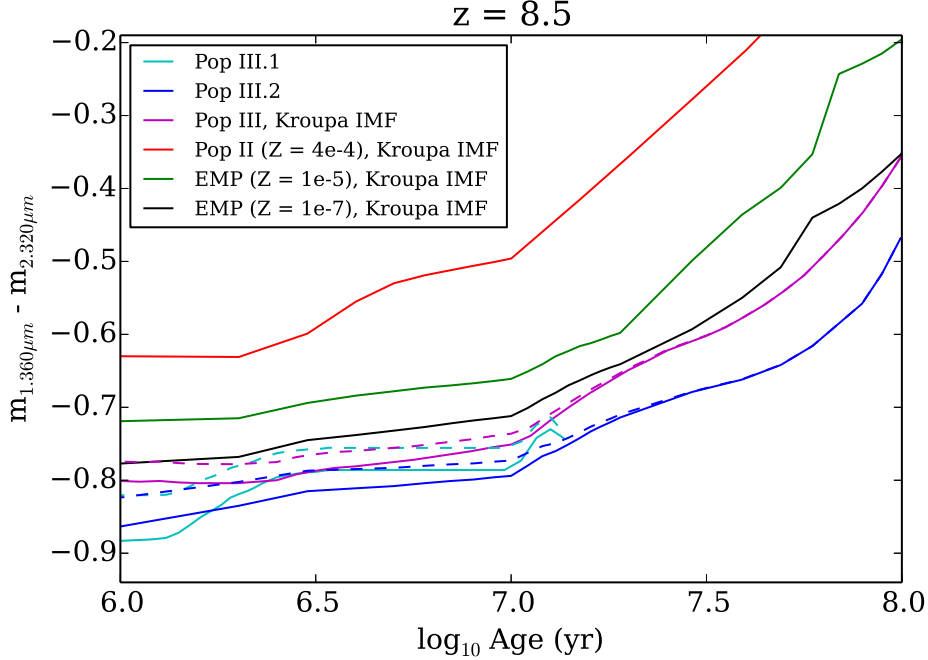


Figure 18: Assuming Kroupa IMF EMP models with $f_{cov} = 0$, only a contribution of $f_{cov} = 0.01$ (dashed lines) to the Pop III galaxy SED can be tolerated before the Pop III IMF signature is effectively lost. Also worth noting, is that anything < -0.7 at 1 Myr would be a *primordial star cluster* (i.e. EMP or Pop III), and a $f_{cov} = 0.01$ contribution applied to the EMP SED would still most likely retain this signature near -0.7 . However, if EMP galaxies are not a factor to consider, a higher fraction might be tolerable, as will be shown in section 2.5.

2.4.1 The drawbacks of a 3σ S/N

A final detail to consider when it comes to applying this method to the WISH UDS survey, is the rather low S/N that can be attained in the observation time allotted, and this produces significant uncertainties when analysing the data. This uncertainty, or error, can be estimated using eq. (5) and (6).

$$\delta m = 2.5 \log_{10} \left(1 + (S/N)^{-1} \right) \quad (5)$$

$$\delta m_{m_1 - m_2} = \sqrt{\delta m_1^2 + \delta m_2^2} \quad (6)$$

The calculation for WISH is trivial, and results in an uncertainty of $\delta m_{tot} = 0.44$ for all colour combinations, assuming the same S/N. Given that $\Delta m_{max} \lesssim 0.20$ in e.g. Fig. 6, not to mention the small margins you end up with when EMP galaxies and nebular contribution are considered, this is clearly an issue, and also a reason for why JWST is critical to the

overall success of this method. If one were to calculate, with an *exposure time calculator* (ETC)⁵, the detection limit at the same *exposure time* (ET \sim 13h, using the $1.360\mu\text{m}$ filter) for WISH at 20σ S/N – resulting in $\delta m = 0.075$ (see section 2.5.1) – would be 26 mag instead of 28 mag. Fortunately, while the uncertainty at 28 mag makes it neigh impossible to say for sure what you have found photometrically, Pop III galaxies should have a visually distinct morphology (appearance) when gravitationally lensed, compared to other lensed photometrically similar galaxies.

An unlensed Pop III galaxy would appear as a mostly reddish blob, with maybe some purple tints in the centre. However, if the same galaxy is strongly lensed, the reddish blob, i.e. the surrounding nebular gas, should become very drawn out and diffuse, while the hot, blue cluster of Pop III stars in the galaxy are strongly magnified. Therefore, due to the morphological differences, the large uncertainties caused by the low S/N will not necessarily yield a lot of false-positives, but rather just make it much more difficult to draw any reliable conclusions concerning the Pop III IMF.

2.5 Final JWST/NIRCam results

If EMP galaxies prove numerous enough that they interfere significantly with this method of detection, then as has been shown above, barely a percent of nebular contribution is tolerable. But what if galaxies dominated by these EMP stars turn out to be completely absent in the survey, or simply rare enough that they do not pose a problem?

In that case we are back to the circumstances encountered in e.g. Fig. 6 (WISH) or Fig. 9 (JWST/NIRCam), where regular Pop I/II stars represent the ‘competition’, as it were. In this situation, a higher fraction of f_{cov} could be tolerated, before distinguishing between IMFs becomes unreliable, as illustrated in Fig. 19 ($f_{cov} = 0.02$) and Fig. 20 ($f_{cov} = 0.04$). The latter shows that a $\sim 4\%$ contribution is probably the highest fraction tolerated by the method, using the $m_{F150W} - m_{F277W}$ colour. This might not seem like much of an improvement over the situation in the previous section, but it is still significant, and more interesting still is that the $m_{F150W} - m_{F200W}$ colour, while perhaps not useful at no or low nebular contribution could be of some use at $f_{cov} > 0.04$.

Under the circumstances of Fig. 18, the first colour combination did not prove to be a better tool than the second one, but as shown in Fig. 21, it might be an option at a higher f_{cov} , displaying a tolerance of up to a $\sim 8\%$ nebular contribution. While the third colour combination still remains the least favourable choice, this indicates that first combination might be useful under some conditions due to a lower sensitivity to higher levels of nebular contributions to the overall SED.

⁵WISH ETC: <http://optik2.mtk.nao.ac.jp/kiyoyabe/WISH/ETC/ETC.py>

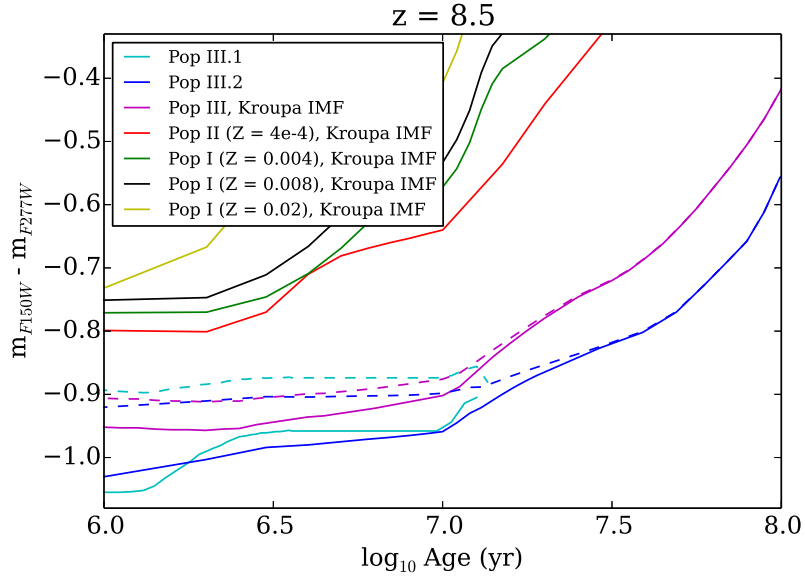


Figure 19: The JWST/NIRCam $m_{F150W} - m_{F277W}$ colour with $f_{cov} = 0.02$ (dashed lines), showing that a 2% nebular coverage should still allow for a clear distinction of the IMF.

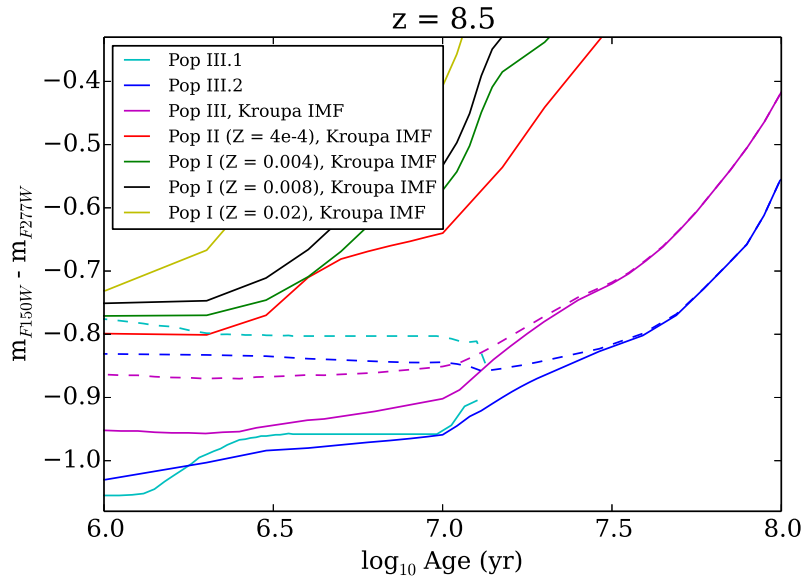


Figure 20: The JWST/NIRCam $m_{F150W} - m_{F277W}$ colour with $f_{cov} = 0.04$ (dashed lines), which can be seen as a rough upper limit of the contribution that can be tolerated under these circumstances.

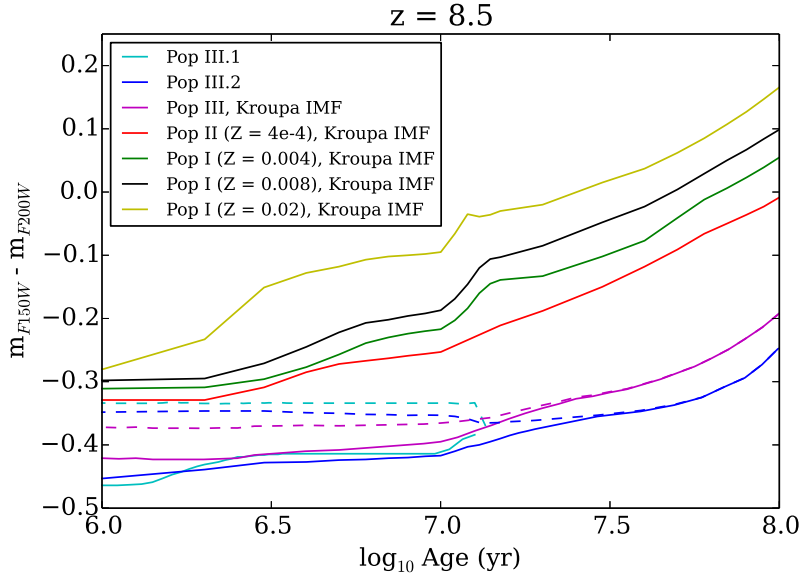


Figure 21: The JWST/NIRCam $m_{F150W} - m_{F200W}$ colour with $f_{cov} = 0.08$ (dashed lines), indicating that the first colour combination could prove useful at a higher fraction of f_{cov} , than what is tolerated by the second colour combination.

2.5.1 Improving the measurements

While WISH will be dedicated to the UDS survey for ~ 4 years and as a result be 'stuck' at 3σ S/N, to obtain a 28 mag detection limit, JWST will be more 'freely' used at whatever objects it observes. As such, the ET can be varied to reach other detection limits and/or different S/Ns. Since the relationship between ET and S/N is not linear, a doubling in ET does not result in twice the S/N, and as was mentioned earlier, you instead pay an ever increasing cost in longer ET when trying to push the detection limit towards fainter objects, or higher precision.

With the ability to vary the ET, it is reasonably easy to investigate what is required for a better S/N at 28 mag in the NIRCam system, using the JWST ETC⁶. While WISH requires ~ 13 hours to reach 28 mag at 3σ for the $1.360\mu\text{m}$ filter, JWST can attain this in < 10 minutes for F150W. This really illustrates the spectacular ability of JWST to obtain a higher precision in a much more reasonable amount of time.

Using the ETC, 10σ is found to be reachable in under an hour for the JWST filters involved in this work, resulting in $\delta m_{tot} = 0.146$ (eq. (5) & (6)) - 1 hour of exposure time is really not much, so I think we can afford a little more. Pushing the S/N to 20σ , at the cost of < 3.5 hours of ET, leaves us with $\delta m_{tot} = 0.075$. Now, it would be possible to go even higher,

⁶ JWST prototype ETC: <http://jwstetc.stsci.edu/etc/input/nircam/imaging/>

say to a S/N of $50\sigma \rightarrow \delta m_{tot} = 0.038$, but at the cost of ~ 14 hours of ET.

A 20σ S/N yields a good compromise between ET and measurement reliability, while allowing the survey of more potential candidates than if a longer ET was used. It is also worth mentioning, that if a detection limit of 29 mag is desired, the ET required for 20σ S/N increases seven fold, to ~ 20 h.

3 Discussion

This work, utilizing models generated from the Yggdrasil population synthesis code, presents a method that could very well be successful in detecting and discerning the stellar IMF of the very first galaxies. There are, however, significant complicating factors and possible limitations, such as what the probability is to find Pop III galaxies with the 'right' combination of sufficiently high stellar mass, and magnification boost due to gravitational lensing, that is required for detection with WISH and JWST. Before discussing that however, I present a brief summary of the method.

- It is possible, as shown in section 2.1, to photometrically distinguish a Pop III IMF from Pop I/II, given a stellar population mass and strong lensing effect that brings them within the detection limits of WISH. The same method is also equally viable for JWST/NIRCam, at roughly the same wavelengths and redshifts, allowing more precise measurements.
- The inclusion of EMP galaxies in the analysis shows that they would greatly complicate the process, being almost impossible to distinguish from Pop III galaxies – unless the EMP stars follow a Kroupa (2001) IMF, as shown in section 2.3 & 2.4.
- The contributions of nebular gas emissions to the overall Pop III galaxy SED can quickly distort the unique photometric signature of Pop III IMFs, even at just a few percent of nebular coverage, as shown in section 2.2, 2.4 & 2.5.
- The WISH UDS survey presents us with a very low S/N, which leads to greater uncertainty when trying to distinguish the Pop III IMF. Fortunately JWST/NIRCam can offer significantly more detailed surveys within a very reasonable ET.

For all the apparent potential of the model, the success of its use, under the conditions presented by the WISH UDS and follow-up observations by JWST at 28 mag, rely mainly on two parameters about which we know much less than we would like to. On one hand, there is the matter of the

stellar population mass of a potential Pop III galaxy. This value is determined by how efficiently stars form from baryonic gas in a CDM halo, and the most optimistic estimate of the *star formation efficiency* (SFE) in these first galaxies is found in the work of Safranek-Shrader et al. (2012). They estimate that, at most, $\sim 0.1\%$ of the baryonic gas in the halo will collapse to form Pop III stars. Now, given that the baryonic content of these CDM halos is assumed to be equal to the cosmic average, $\sim 15\%$, this means that for a $10^8 M_\odot$ halo we end up $1.5 \times 10^7 M_\odot$ of baryonic matter, 0.1% of which will form a stellar population mass of $1.5 \times 10^4 M_\odot$.

Unfortunately, a Pop III galaxy with this stellar mass would only be detectable with the help of a gravitational lens providing a $\mu \sim 3000$ magnification. As shown in Fig. 3, this corresponds to a probability of 9.28×10^{-10} for finding a source at $z = 8.5$ with this magnification. If we from Fig. 2 estimate that there are 150 Pop III galaxies per arcmin² at $z = 8.5$, this means there are $100 \text{deg}^2 \times 150 = 3.6 \times 10^5 \text{arcmin}^2 \times 150 = 5.4 \times 10^7$ Pop III galaxies within the field of the WISH UDS. Through further calculations, one ends up with a ~ 0.05 probability of finding a single Pop III galaxy, that has attained a magnification of $\mu > 3000$, in the UDS survey. If we instead look at $\mu > 1000$, the probability to find one Pop III galaxy with this magnification increases to ~ 0.35 . For $\mu \gtrsim 500$, the probability of which can be extrapolated from Fig. 3 (based on the standard result $P(> \mu) \propto \mu^{-2}$), it increases to ~ 0.80 , which would require a stellar population mass of $\sim 1.2 \times 10^5 M_\odot$.

While our understanding regarding extreme gravitational lensing will improve in the coming years leading up to the launch of JWST, and hopefully the launch of WISH, it is clear that given these current estimates, the odds are not good for finding a Pop III galaxy, with a magnification of $\mu > 3000$ in the UDS. As previously mentioned in section 1.5, a stellar population mass of $\sim 6 \times 10^4 M_\odot$ in combination with $\mu > 1000$, would be required to bring the Pop III galaxy within the detection limits, with a $\sim 35\%$ chance of one such object being contained in the UDS. But this stellar mass would in turn require, according to the SFE from Safranek-Shrader et al. (2012), a halo mass of $4 \times 10^8 M_\odot$. The plot of the Pop III galaxy population density shown in Fig. 2 was created assuming a halo mass of $10^7 - 10^8 M_\odot$. So if even higher halo masses are required, then such halos might give rise to completely different predictions regarding the number density of Pop III galaxies at the relevant redshifts. As such, given the data at hand, it is difficult to offer further estimates regarding the likelihood of finding a Pop III galaxy during the 'right' circumstances. So as it looks now, (far) higher stellar masses than currently predicted would be required, at the more likely magnification of $\mu > 100$, which guarantees more than one such Pop III galaxy in the UDS.

With that being said, there have been observational claims pointing to the fact that higher stellar masses (which would indicate a higher SFE

and/or larger halo mass) than currently predicted, could very well be possible at high redshifts. A recent such example is an article by Kashikawa et al. (2012), where they have found an object/galaxy at $z = 6.5$, with a stellar mass of $10^6 - 10^7 M_{\odot}$, composed of what they estimate to be metal-free and metal-poor stars. Whether these stars are in fact entirely metal free, i.e. like Pop III stars, or simply some form of EMP or Pop II stars is unclear. But if they are in fact Pop III stars, it would indicate that current simulations concerning halo mass and/or SFE at high redshifts are flawed.

In principle, this method should be able to detect a Pop III galaxy, and allows us to discern something about the IMF of the stars therein. If it will actually be applicable under the right conditions, only time will tell.

Acknowledgements

Finally, here at the completion of this thesis, I would first like to give a big and heartfelt Thank you! to my supervisor Erik Zackrisson for the continued support he has provided during these past two months. In addition to the drafts he has read through and commented extensively, his patience and understanding has helped me to grasp things that I previously was completely unfamiliar with. In the process, I have also gained an understanding of his own field of research, as it is (naturally) closely related to the work I have presented here.

I would also like to thank everyone at the Department of Astronomy at Stockholm University, Albanova, for being so very welcoming to all their third year bachelor students - it was always a pleasure to hang around up on "Plan 6" - and we were never met with anything but friendly faces, and well, "fika". I look forward to spending the next two years at Albanova for my masters degree!

References

- Abel, T., Bryan, G. L. & Norman, M. L. 2002, [Sci 295, 93](#)
- Asplund, M., Grevesse, N., Sauval, A. J. & Scott, P. 2009, [A&A 47, 481](#)
- Barkana, R. & Loeb, A. 2001, [PhR 349, 125](#)
- Bromm, V., Coppi, P. S. & Larson, R. B. 1999, [ApJ 527, 5](#)
- Bromm, V., Yoshida, N., Hernquist, L. & McKee, C. E. 2009, [Natur 459, 49](#)
- Chatzopoulos, E., & Wheeler, J. C. 2012, [ApJ 748, 42](#)
- Chen, K.-J., Helger, A., Woosley, S., Almgren, A. & Whalen, D. J. 2014, [arXiv:1402.5960](#)
- Choi, J.-Y. et al. 2013, [ApJ 768, 129](#)
- Greif, T. H. et al. 2008, [IAUS 255, 33](#)
- Greif, T. H., Glover, S. C. O., Bromm, V. & Klessen, R. S. 2010 [ApJ 716, 510](#)
- Gunn, J. E. & Peterson, B. A. 1965 [ApJ 142, 1633](#)
- Hoekstra, H., Bartelmann, M., Dahle, H., Israel, H., Limousin, M. & Meneghetti, M. 2013, [SSRv 177, 50](#)
- Hosokawa, T., Omukai, K., Yoshida, N. & Yorke, H. 2011, [Sci 334, 1250](#)
- Inoue, A. K., Shimizu, I., Iwata, I. & Masayuki, T. 2014, [arXiv:1402.0677](#)
- Joggerst, C. C., Almgren, A., Bell, J., Heger, A., Whalen, D. & Woosley, S. E. 2010, [ApJ 709, 11](#)
- Karlsson, T. 2009, [IAUS 254, 343](#)
- Karlsson, T., Bromm, V. & Bland-Hawthorn, J. 2013, [RvMP 85, 809](#)
- Kashikawa, N. et al. 2012, [ApJ 761, 85](#)
- Komiya, Y., Suda, T. & Fujimoto, M. 2013, [arXiv:1312.5069](#)
- Kitayama, T. & Yoshida, N. 2005, [ApJ 630, 675](#)
- Kroupa, P. 2000, [ASPC 228, 187](#)
- Kroupa, P. 2001, [MNRAS 322, 231](#)
- Leitherer et al. 1999 [ApJS 123, 3](#)
- Oguri, M., Rusu, C. E. & Falco, E.E 2014, [MNRAS 439, 2494](#)
- Madau, P. 1995, [ApJ 441, 18](#)
- Mori, M., Ferrara, A. & Madau, P. 2002, [ApJ 571, 40](#)
- Mortlock, D. J. et al. 2011, [Natur 474, 616](#)
- Nakamura, F. & Umemura, M. 2001, [ApJ 548, 19](#)
- O'Shea, B. W. & Norman, M. L. 2007, [ApJ 654, 66](#)

- Planck Collaboration, submitted 2013 to A&A, [arXiv:1303.5062v1](#)
- Raiter, A., Schaerer, D. & Fosbury, R. A. E. 2010, [A&A 523, 64](#)
- Ritter, J. S., Safrank-Shrader, C., Gnat, O., Molosavljević, M.
& Bromm, V. 2012, [ApJ 761, 56](#)
- Rydberg, C., Zackrisson, E., Lundqvist, P. & Scott, P. 2013,
[MNRAS 429, 3658](#)
- Safrank-Shrader, C. et al. 2012, [MNRAS 426, 1159](#)
- Schaerer, D. 2002, [A&A 382, 28](#)
- Sharon, K., Ofek E. O., Smith, G. P., Broadhurst, T., Maoz, D.,
Kochanek, C. S., Oguri, M., Suto, Y., Inada, N. & Falco, E. E. 2005,
[ApJ 629, 73](#)
- Stacy, A. & Bromm, V. 2014, [ApJ 785, 73](#)
- Tanaka, T. L. & Li, M. 2014, [MNRAS 439,1092](#)
- Vazquez, G. A. & Leitherer, C. 2005, [ApJ 621, 695](#)
- Whalen, D. J. & Fryer, C. L. 2012, [ApJ 756, 19](#)
- Yong, D. et al. 2013, [ApJ 762, 27](#)
- Yoshida, N., Oh, S. P., Kitayama, T. & Hernquist, L. 2007, [ApJ 663, 687](#)
- Zackrisson, E., Rydberg, C.-E., Schaerer, D., Östlin, G. & Tuli, M. 2011,
[ApJ 740, 13](#)
- Zackrisson, E., Zitrin, A., Trenti, M., Rydberg, C.-E., Guaita, L., Schaerer,
D., Broadhurst, T., Östlin, G. & Ström, T. 2012, [MNRAS 427, 2213](#)

Appendix: Python Code Example

Here I present an example of the python code that has been used for this work, utilizing the relatively new (and extremely useful) IP(y)Notebook interface. The code below (which would reproduce Fig. 20) follows the process of data preparation, selection, manipulation and finally plotting, that has been used for the WISH and JWST data. The code has evolved as work progressed, and the example listed is limited to the F150W - F277W combination, but the data handling for other filters or models (e.g. EMP) is more or less analogous.

```
# Packages and settings
%pylab inline
# Import numpy for some mathematical operation
import numpy as np
# Import pylab for plotting
import pylab as pl
pl.rcParams['figure.figsize'] = (7.0, 4.9)

#####
# Raw data import for JWST (F444W column excluded)
# Format: AAAAx10 lists
# f_cov_0
PopIII10 = loadtxt("JWST.PopIII.1.fc0.txt", skiprows =1, usecols =
    (0,1,2,3,4,5,6,7,8,9)) #8723 rows
PopIII20 = loadtxt("JWST.PopIII.2.fc0.txt", skiprows =1, usecols =
    (0,1,2,3,4,5,6,7,8,9)) #3294 rows
PopIIIk0 = loadtxt("JWST.PopIII.k.fc0.txt", skiprows =1, usecols =
    (0,1,2,3,4,5,6,7,8,9)) #6771 rows

Z00040 = loadtxt("JWST.Z0.0004.fc0.txt", skiprows =1, usecols =
    (0,1,2,3,4,5,6,7,8,9)) #2562 rows
Z0040 = loadtxt("JWST.Z0.004.fc0.txt", skiprows =1, usecols =
    (0,1,2,3,4,5,6,7,8,9)) #2867 rows
Z0080 = loadtxt("JWST.Z0.008.fc0.txt", skiprows =1, usecols =
    (0,1,2,3,4,5,6,7,8,9)) #2806 rows
Z020 = loadtxt("JWST.Z0.02.fc0.txt", skiprows =1, usecols =
    (0,1,2,3,4,5,6,7,8,9)) #2867 rows

# f_cov_1
PopIII11 = loadtxt("JWST.PopIII.1.fc1.txt", skiprows =1, usecols =
    (0,1,2,3,4,5,6,7,8,9)) #2867 rows
PopIII21 = loadtxt("JWST.PopIII.2.fc1.txt", skiprows =1, usecols =
    (0,1,2,3,4,5,6,7,8,9)) #3294 rows
PopIIIk1 = loadtxt("JWST.PopIII.k.fc1.txt", skiprows =1, usecols =
    (0,1,2,3,4,5,6,7,8,9)) #6771 rows

Z00041 = loadtxt("JWST.Z0.0004.fc1.txt", skiprows =1, usecols =
    (0,1,2,3,4,5,6,7,8,9)) #2135 rows
Z0041 = loadtxt("JWST.Z0.004.fc1.txt", skiprows =1, usecols =
    (0,1,2,3,4,5,6,7,8,9)) #2196 rows
Z0081 = loadtxt("JWST.Z0.008.fc1.txt", skiprows =1, usecols =
    (0,1,2,3,4,5,6,7,8,9)) #2562 rows
Z021 = loadtxt("JWST.Z0.02.fc1.txt", skiprows =1, usecols =
    (0,1,2,3,4,5,6,7,8,9)) #2867 rows
```

```
#####  
# f_cov_0 data lists are of different length, bloated with rows  
# containing 999 magnitude (0 Flux) (F070W also removed entirely).  
# Have to first remove these, to be able to do calculations using flux  
#  
# _p for "purged"  
PopIII10_p = PopIII10[(PopIII10[:,5]<900)]; PopIII11_p = PopIII11[(  
    PopIII11[:,5]<900)]  
PopIII20_p = PopIII20[(PopIII20[:,5]<900)]; PopIII21_p = PopIII21[(  
    PopIII21[:,5]<900)]  
PopIIIk0_p = PopIIIk0[(PopIIIk0[:,5]<900)]; PopIIIk1_p = PopIIIk1[(  
    PopIIIk1[:,5]<900)]  
  
# For Z00040, Z0040, Z0080, there are superfluous rows due to the fact  
# that the code responsible for calculating  
# nebular contribution can't handle too high ages. These have to be  
# removed from f_cov_0 for the lists to be compatible.  
Z00040_p = Z00040[(Z00040[:,5]<900) & (Z00040[:,1]<8e9)]; Z00041_p =  
    Z00041[(Z00041[:,5]<900)]  
Z0040_p = Z0040[(Z0040[:,5]<900) & (Z0040[:,1]<4e9)]; Z0041_p = Z0041  
    [(Z0041[:,5]<900)]  
Z0080_p = Z0080[(Z0080[:,5]<900) & (Z0080[:,1]<1e10)]; Z0081_p = Z0081  
    [(Z0081[:,5]<900)]  
Z020_p = Z020[(Z020[:,5]<900)]; Z021_p = Z021[(Z021[:,5]<900)]  
  
# Only 100% Nebular contribution. Includes mass correction if  
# magnitudes are normalized to masses other than 1e6.  
PopIII1_pfnneb = ((10**(-0.4*(PopIII11_p[:,5:10]))) / 1e6 - 10**(-0.4*(  
    PopIII10_p[:,5:10])))  
PopIII2_pfnneb = ((10**(-0.4*(PopIII21_p[:,5:10]))) / 1e6 - 10**(-0.4*(  
    PopIII20_p[:,5:10])))  
PopIIIk_pfnneb = ((10**(-0.4*(PopIIIk1_p[:,5:10]))) / 1e6 - 10**(-0.4*(  
    PopIIIk0_p[:,5:10])))  
Z0004_pfnneb = (10**(-0.4*(Z00041_p[:,5:10])) - 10**(-0.4*(Z00040_p  
   [:,5:10])))  
Z004_pfnneb = (10**(-0.4*(Z0041_p[:,5:10])) - 10**(-0.4*(Z0040_p[:,5:10]  
    )))  
Z008_pfnneb = (10**(-0.4*(Z0081_p[:,5:10])) - 10**(-0.4*(Z0080_p[:,5:10]  
    )))  
Z02_pfnneb = (10**(-0.4*(Z021_p[:,5:10])) - 10**(-0.4*(Z020_p[:,5:10]  
    )))  
  
# Original first 4 columns + filter columns = 0, will need these later  
# ...  
PopIII10_null = np.hstack((PopIII10_p[:,0:5], (np.zeros((PopIII10_p  
   [:,0:4].shape[0],5))))))  
PopIII20_null = np.hstack((PopIII20_p[:,0:5], (np.zeros((PopIII20_p  
   [:,0:4].shape[0],5))))))  
PopIIIk0_null = np.hstack((PopIIIk0_p[:,0:5], (np.zeros((PopIIIk0_p  
   [:,0:4].shape[0],5))))))  
Z00040_null = np.hstack((Z00040_p[:,0:5], (np.zeros((Z00040_p[:,0:4].  
    shape[0],5))))))  
Z0040_null = np.hstack((Z0040_p[:,0:5], (np.zeros((Z0040_p[:,0:4].shape  
    [0],5))))))  
Z0080_null = np.hstack((Z0080_p[:,0:5], (np.zeros((Z0080_p[:,0:4].shape  
    [0],5))))))  
Z020_null = np.hstack((Z020_p[:,0:5], (np.zeros((Z020_p[:,0:4].shape  
    [0],5))))))
```

```
#####  
### JWST filters F150W-F277W. Max redshift for this combination: 8.5.  
    Filter 3 (F150W) cuts out at z~8.5.  
z1 = 850  
z = z1/1e2; # Workaround for automatic file naming  
m1 = 6; m2 = 8 # Initial filters  
  
# Define function for plotting f_cov = 0. Selects rows with relevant  
  redshift and double checks flux =| 0.  
def plot_table1(srclist1, z, m1, m2, color = 'k'):  
    slice = srclist1[(srclist1[:,0]==z) & (srclist1[:, 6] < 900)]  
    pl.plot(log10(slice[:, 1]), slice[:, m1] - slice[:, m2], '--',  
            color = color)  
  
srclists1 = [PopIII10, PopIII20, PopIIIk0, Z00040, Z0040, Z0080, Z020]  
  
### Calculate the nebular contribution within the the same cell  
F1 = 4 # Nebular contribution scaling factor, 100 = 1.0  
F = F1/1e2 # Workaround for automatic file naming  
  
# New magnitudes with nebular contribution  
PopIII10_m = -2.5*log10((10**(-0.4*(PopIII10_p[:,5:10]))) + F*  
    PopIII1_pfnneb)  
PopIII20_m = -2.5*log10((10**(-0.4*(PopIII20_p[:,5:10]))) + F*  
    PopIII2_pfnneb)  
PopIIIk0_m = -2.5*log10((10**(-0.4*(PopIIIk0_p[:,5:10]))) + F*  
    PopIIIk_pfnneb)  
Z00040_m = -2.5*log10((10**(-0.4*(Z00040_p[:,5:10]))) + F*Z0004_pfnneb)  
Z0040_m = -2.5*log10((10**(-0.4*(Z0040_p[:,5:10]))) + F*Z004_pfnneb)  
Z0080_m = -2.5*log10((10**(-0.4*(Z0080_p[:,5:10]))) + F*Z008_pfnneb)  
Z020_m = -2.5*log10((10**(-0.4*(Z020_p[:,5:10]))) + F*Z02_pfnneb)  
  
# Recombine with the other columns, ready to plot  
PopIII10_n = PopIII10_null + (np.hstack((np.zeros((PopIII10_m.shape  
    [0],5)),PopIII10_m)))  
PopIII20_n = PopIII20_null + (np.hstack((np.zeros((PopIII20_m.shape  
    [0],5)),PopIII20_m)))  
PopIIIk0_n = PopIIIk0_null + (np.hstack((np.zeros((PopIIIk0_m.shape  
    [0],5)),PopIIIk0_m)))  
Z00040_n = Z00040_null + (np.hstack((np.zeros((Z00040_m.shape[0],5)),  
    Z00040_m)))  
Z0040_n = Z0040_null + (np.hstack((np.zeros((Z0040_m.shape[0],5)),  
    Z0040_m)))  
Z0080_n = Z0080_null + (np.hstack((np.zeros((Z0080_m.shape[0],5)),  
    Z0080_m)))  
Z020_n = Z020_null + (np.hstack((np.zeros((Z020_m.shape[0],5)),Z020_m  
    )))  
  
### Define function for plotting variable f_cov  
  
def plot_table2(srclist2, z, m1, m2, color = 'k'):  
    slice = srclist2[(srclist2[:,0]==z) & (srclist2[:, 5] < 900)]  
    pl.plot(log10(slice[:, 1]), slice[:, m1] - slice[:, m2], '--',  
            color = color)  
  
srclists2 = [PopIII10_n, PopIII20_n, PopIIIk0_n]  
  
### Plot away!
```

```
figure(1)

colors = ['y', 'k', 'g', 'r', 'm', 'b', 'c']
for srclist1 in srclists1:
    plot_table1(srclist1, z, m1, m2, color=colors.pop())

colors = ['m', 'b', 'c']
for srclist2 in srclists2:
    plot_table2(srclist2, z, m1, m2, color=colors.pop())

pl.xlabel('log$_{10}$ Age (yr)')
pl.ylabel('m$_{F150W}$ - m$_{F277W}$')
legend( ( ('Pop III.1'), ('Pop III.2'), ('Pop III, Kroupa IMF'), ('Pop
    II (Z = 4e-4), Kroupa IMF'), ('Pop I (Z = 0.004), Kroupa IMF'), ('
    Pop I (Z = 0.008), Kroupa IMF'), ('Pop I (Z = 0.02), Kroupa IMF')
    ), loc='upper left', fontsize='10')
axis([6, 8, -1.08, -0.33])

title('z = {0}'.format(z))
pl.savefig('JWST.(F150W-F277W).z{0}.dashed_f_neb{1}%.eps'.format(z1, F1
))
#pl.savefig('JWST.(F150W-F277W).z{0}.dashed_f_neb{1}%.png'.format(z1,
    F1))
```